University of California at Berkeley
Department of Electrical Engineering and Computer Sciences

Memo

To: Prof. T Van Duzer

From: Mark Jeffery

CC: Steve Whiteley

Date: 08/24/98

Re: Verification of WRspice thermal noise simulation accuracy

---

Thermal noise has been incorporated into the WRspice commercial Josephson circuit simulator. The noise is implemented at the source code level, and therefore the WRspice simulator should have a speed advantage over other methods that add noise from an external file. However, verification that the noise is correctly implemented in the simulator is important if the results of the simulations are to be used by other laboratories.

Thermal noise, also known as Nyquist or Johnson noise, is modeled in a circuit by random current sources in parallel with each resistor in the circuit. The rms. of these current fluctuations is given by the Nyquist formula

$$i_{rms} = \sqrt{\frac{4KTf_c}{R}} \qquad (1)$$

Where K is Boltzman's constant, T is temperature, R is the resistance, and the cutoff frequency f_c = 1/2Δ where Δ is the spacing between random numbers. If the noise (1) is bandwidth limited, i.e. output from a filter, f_c in Eq. (1) becomes the bandwidth of the filter.

Noise is implemented in WRspice through the gauss function defined in the WRspice file by

```
*@ define noise(r,t,dt,n) gauss(sqrt(4*boltz*t/(r*2*dt)), 0, dt, n)
```

This noise function is then applied in parallel with each Josephson junction and resistor: A typical call to the gauss function is:

```
b1 1 0 4 ybco4 area=0.0625
I10 1 0 noise($Rval, $Temp, $tmin, $whichn)
```

Where the Josephson junction has an intrinsic WRspice model that includes capacitance and R_n

```
.model ybco4 jj(rtype=1,cct=1,icon=10m,vg=28m,delv=2m,
+ icrit=0.16m,r0=$Rnval,rn=$Rnval,cap=0.05p)
```

The spice simulator must calculate circuit transients at time intervals less than Δ. To ensure algorithm stability WRspice interpolates the random noise function between successive Δ spaced time points. Two interpolation schemes are used. The first makes the noise constant at the beginning and end points of each Δ interval. The second noise function is a first order linear interpolation between points. This first noise function therefore consists of square "steps" with step width Δ. This square noise was originally used by Satchel, in part since it is easier to input from an external file into JSIM. However, Jeffery has previously used cubic spline interpolated noise with good results. In general as long as the Δ time scale spacing of the noise is small compared with the time constants in the circuit, the output of the simulation should be independent of the exact form of the input noise function.

Typical noise generated by WRspice is shown in FIG. 1. The top trace is thermal noise on a 20 Ω resistor at 4.2 K, and the bottom trace is the noise at the output of a 10 GHz center frequency, 5 GHz bandwidth filter. The power spectra of the noise (top trace) is shown in Fig. 2. Note that the noise spectral density is approximately flat out to the Nyquist cutoff frequency $f_c = 1/2\Delta$, where for the simulation $\Delta = 5$ ps and therefore $f_c = 100$ GHz. The calculated rms. of the voltage fluctuations for the noise from the simulation data in FIG. 1 is exactly the rms. of the current given by Eq. (1) multiplied by R.

FIG. 3 shows the power spectra with random numbers spaced $\Delta = 5$ ps apart, but with the WRspice calculating at $\Delta/2$ intervals. For this case, the noise function between the Δ random deviates is obtained by a simple linear interpolation. The resulting power spectra is shaped around f_c, due to the higher harmonics generated from the linear interpolation. FIG. 4 and FIG. 5 show the difference in power spectra between using linear interpolated noise and piece-wise constant linear steps. Comparison of the FFT show that the first order linear interpolated noise has significantly reduced higher harmonics, compared to the square noise. Higher order interpolation can almost completely eliminate the higher order harmonics. Finally, FIG. 6 shows the FFT of the noise output from a RLC filter with center frequency 10 GHz, and bandwidth 5 GHz. The FFT demonstrates that the noise is shaped by the filter transfer function.

The WRspice simulator with thermal noise and Josephson junctions has been analyzed in detail. Specifically, I have calculated the rounding of the IV curve due to thermal noise first reported by Ambegaokar and Halperin (AH) in 1969. Comparison with the AH thermal noise rounding is a standard test used to verify Josephson junction simulators including thermal noise and has been used by Tesche and Clarke, and Satchel. Both authors report simulations in good agreement with the AH result.

Prof. Whiteley and I wrote a script program that can run and average the output of a WRspice file, while incrementing the dc current bias. This script was then generalized to run a WRspice deck with various parameters. The AH paper defines the parameter $\gamma = h I_c / 2\pi eKT$, where γ ranges from 0 to infinity. For example, typical γ values are 2, 10, and 40. For a 10 μA I_c junction these values of γ correspond to temperatures of 238 K, 47.79 K, and 11.95 K respectively. A 10 μA junction with a 1 Ω R_n was implemented in WRspice with a thermal noise source and dc current bias. The script then iterated for varying bias currents, and for several values of γ.

FIG. 7 Shows the output from a Josephson junction with a random noise source (bottom trace). The junction is biased at 9 μA and the noise causes the junction phase to switch by multiples of 2 π (these are the random steps in the top trace [π = 3.141 V in the plot]). This junction switching generates voltage spikes that, when averaged, causes the rounding of the IV curve. The junction voltage spikes are buried in the thermal noise of FIG. 7.

FIG. 8 and FIG. 9 show data points calculated by incrementing the bias current for different values of γ, and overlaid on the AH curves calculated from their pseudo analytic formula. The AH curves were

taken from p191 of Vanduzer and Turner.Note that each data point in FIG. 8 is an averaging of output similar to FIG. 7. Each data point in FIG. 8 was therefore calculated by simulating for 50 ns at 1p steps, and averaging the resulting 50,000 data points. The data in FIG. 9 was obtained from a longer simulation time of 100 ns (100,000 averaged simulation points for each point in the plot). Note that the data in FIG. 8 fluctuates around the AH curves, increasing the number of averaged points as in FIG. 9 significantly decreases these fluctuations. The fluctuations about the AH curves are larger for small γ; this corresponds to increased temperature. Note that the data plot in FIG. 9 is almost identical to that given by Tesche and Clarke on p317 Fig. 11(a), and is within a few percent of the original AH values. Higher accuracy can be obtained by increasing the length of the averaged data sets. Identical plots to FIG. 7 and 8 were obtained using linear interpolated or piece-wise constant noise, and the simulations were found to be independent of the cutoff frequency f_c.

The WRspice simulation results are therefore in excellent agreement with the AH results. An overlay of the noise simulation with the plot on p191 of Vanduzer and Turner demonstrates that WRspice noise simulator is accurate to within a few percent. The comparison with the theory of AH is a significant test to demonstrate the validity of the simulator.

Acknowledgement

I would like to gratefully acknowledge S. Whiteley for his help implementing the noise function in WRspice, and assisting with the many questions regarding his spice software.

References

H. Nyquist, *Thermal Agitation of Charge in Conductors*, Phys. Rev. 32., pp110-113, (1928).

S. R. Whiteley, *Josephson Junctions in Spice3*, IEEE Trans Magn., vol 27., no. 2, pp. 2902-2905, March 1991. For more information on WRspice contact S. Whiteley at stevew@srware.com, Phone: (408) 735-8973, FAX: (408) 245-4033.

W. H. Press, B. P. Flannery, S. A. Tekolsky, W. T. Vetterling, *Numerical Recipes in C the Art of Scientific Computing*, Cambridge University Press, New York, (1990) p403

V. Ambegaokar an B. L. Halperin, *Voltage Due to Thermal Noise in the dc Josephson Effect*, Phys. Rev. Lett., Vol 22, No. 25, (1969) pp1364-1366

C. D. Tesche and J. Clarke, *dc SQUID: Noise and Optimization*, Journal of Low Temperature Physics, Vol. 29. Nos. ¾, (1977) pp301-331

J. Satchel, *Stochastic Simulation of SFQ Logic*, IEEE Trans. on Appl. Supercond., vol. 7, No. 2 (1997), pp3315-3318.

T. Van Duzer and C. W. Turner, *Principles of Superconducting Devices and Circuits*, Elsevier, New York, 1981, p191.

Mark Jeffery, *Subquantum Limit Josephson Magnetometry*, Appl. Phys. Lett., **66**, (21), 2897 (1995).

Mark Jeffery, *Analysis of a High Temperature Superconductor Quantum Flux Parametron Operating at 77K*, IEEE Transactions on Applied Superconductivity, Vol. 5 No. 4, 3522 (1995).

SIMPLE RLC CIRCUIT WITH NOISE

$D = \frac{1}{2f_c} \rightarrow f_c = \frac{1}{2D}$

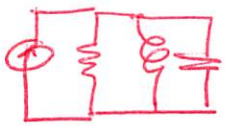

.tran Sp 100n

↑
D

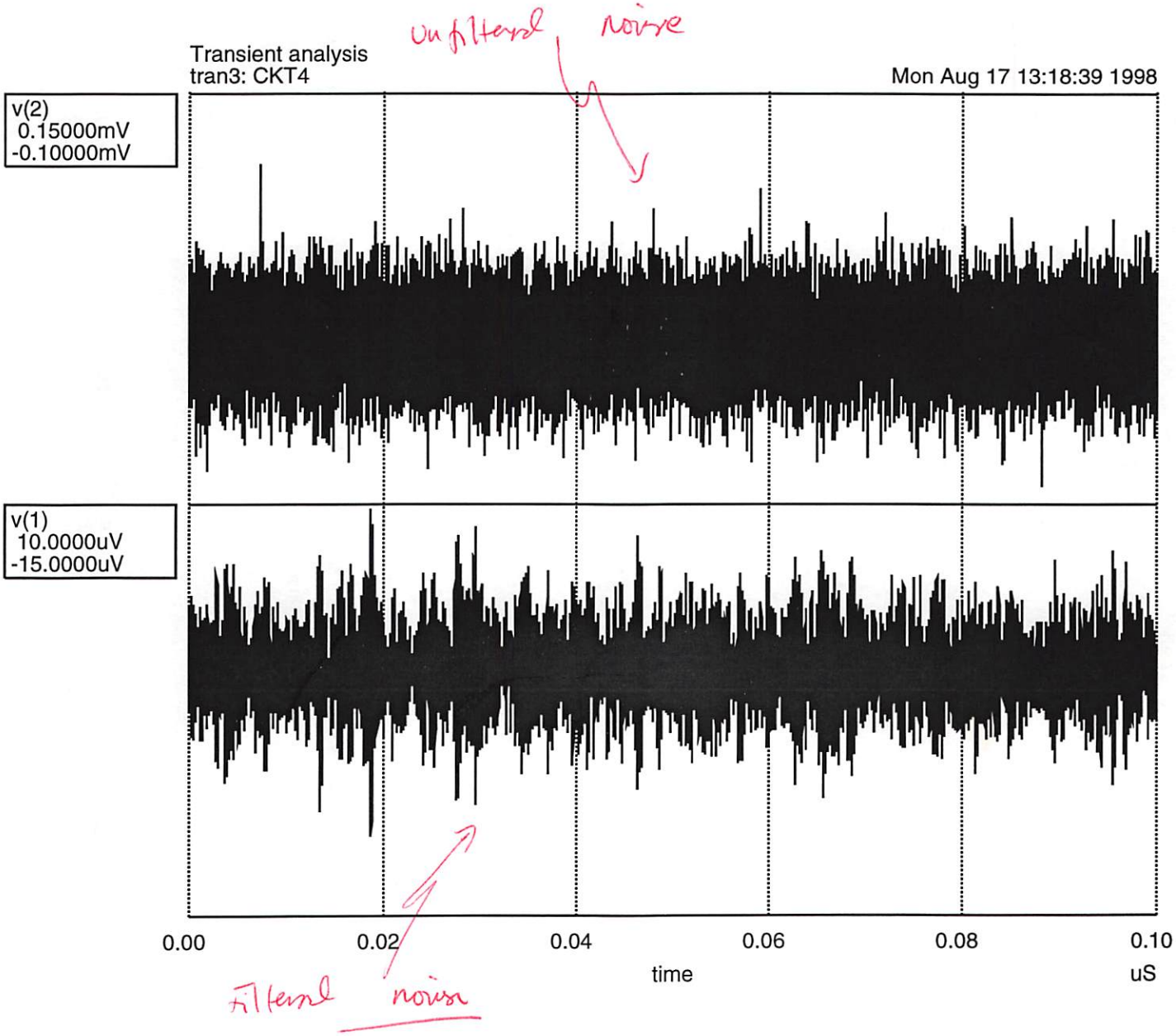

Fig 1.

FFT of unfiltered noise

$D = 5p$ $f_c = \frac{1}{2(5p)} = 100GHz$

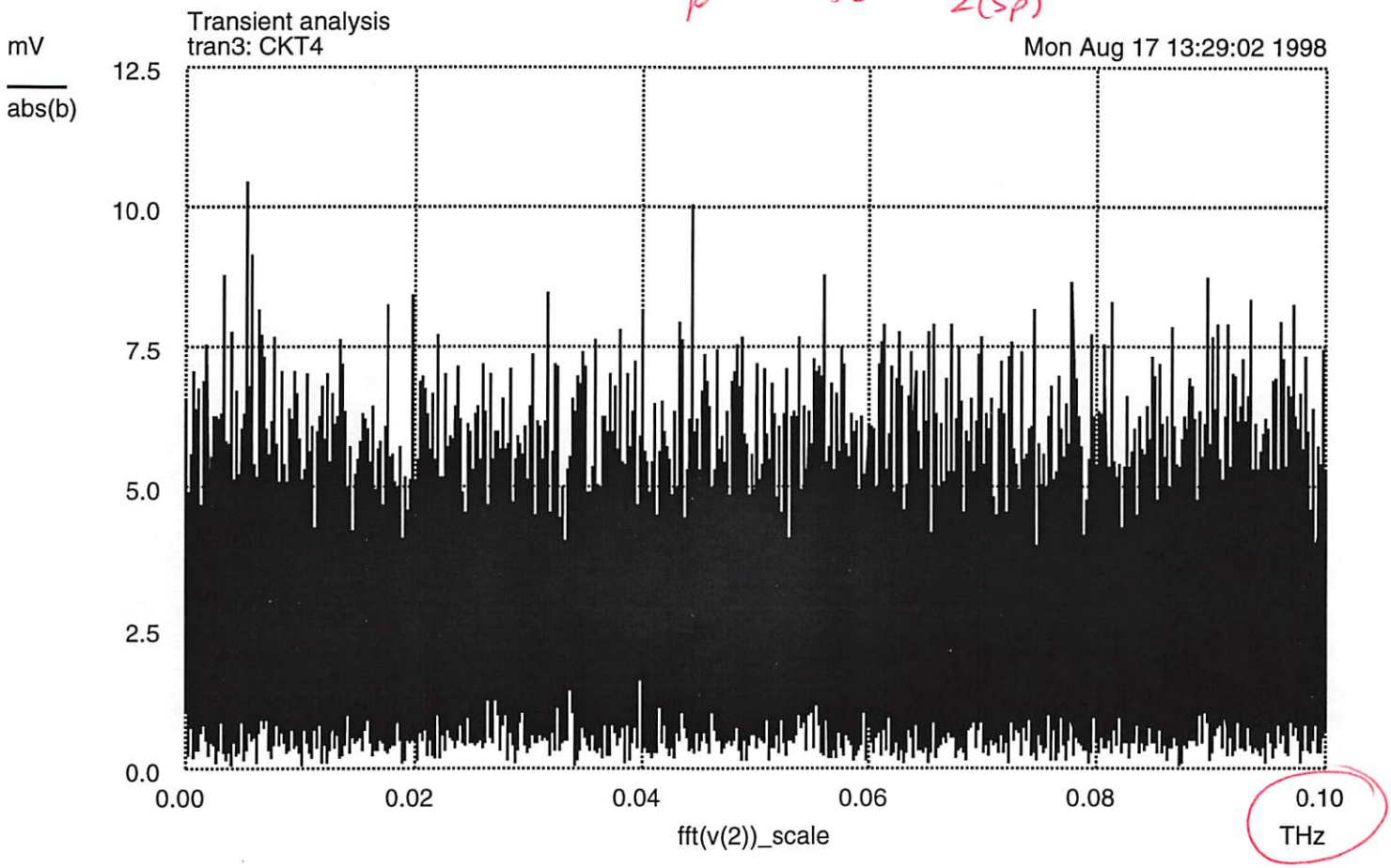

Fig. 2.

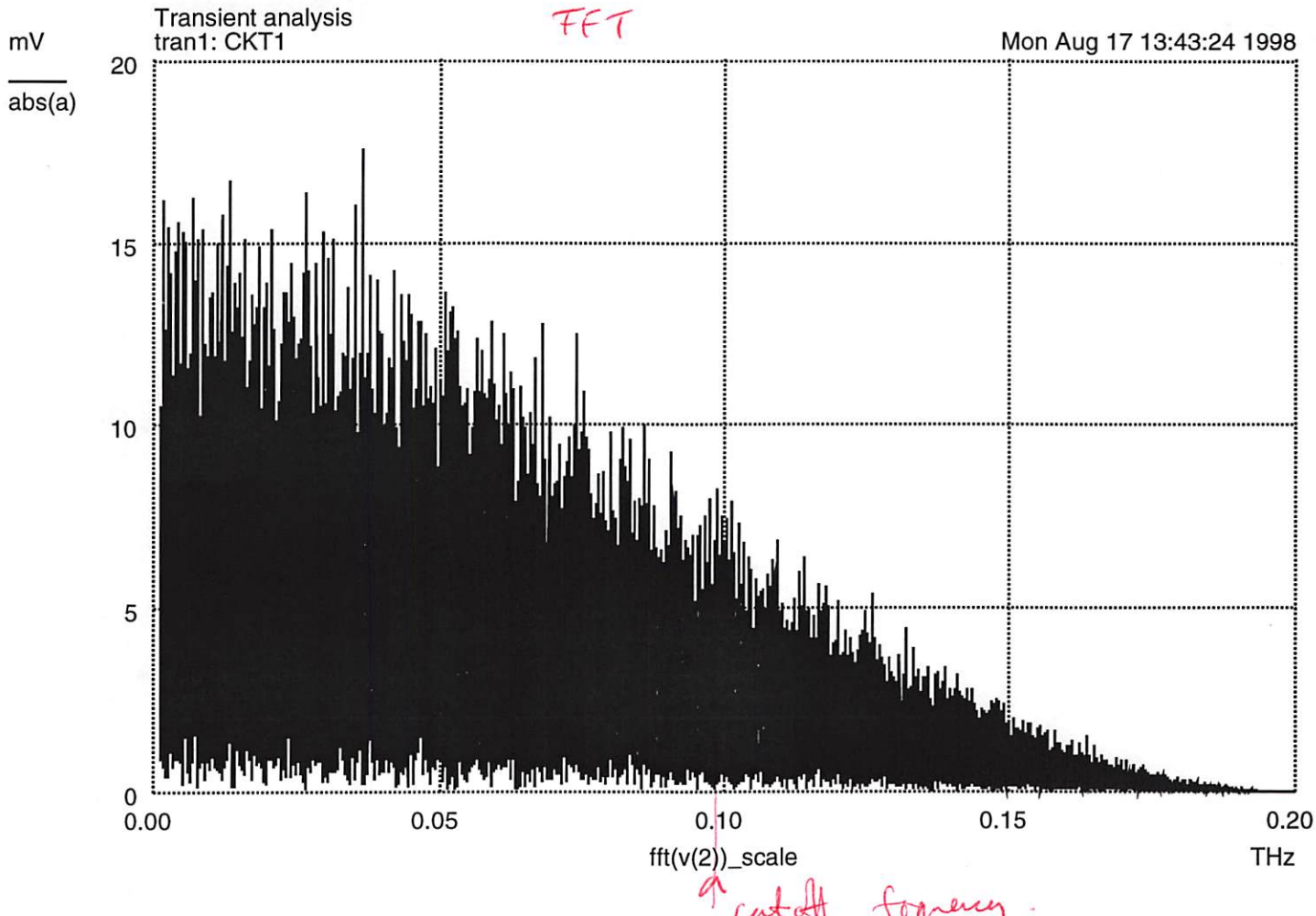

D = 5ps

but step = 2.5ps

Smoothing is due to harmonics or noise.

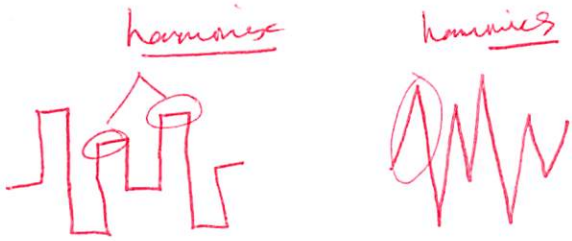

Fig. 3.

FFT : FIRST ORDER INTERPOLATED NOISE

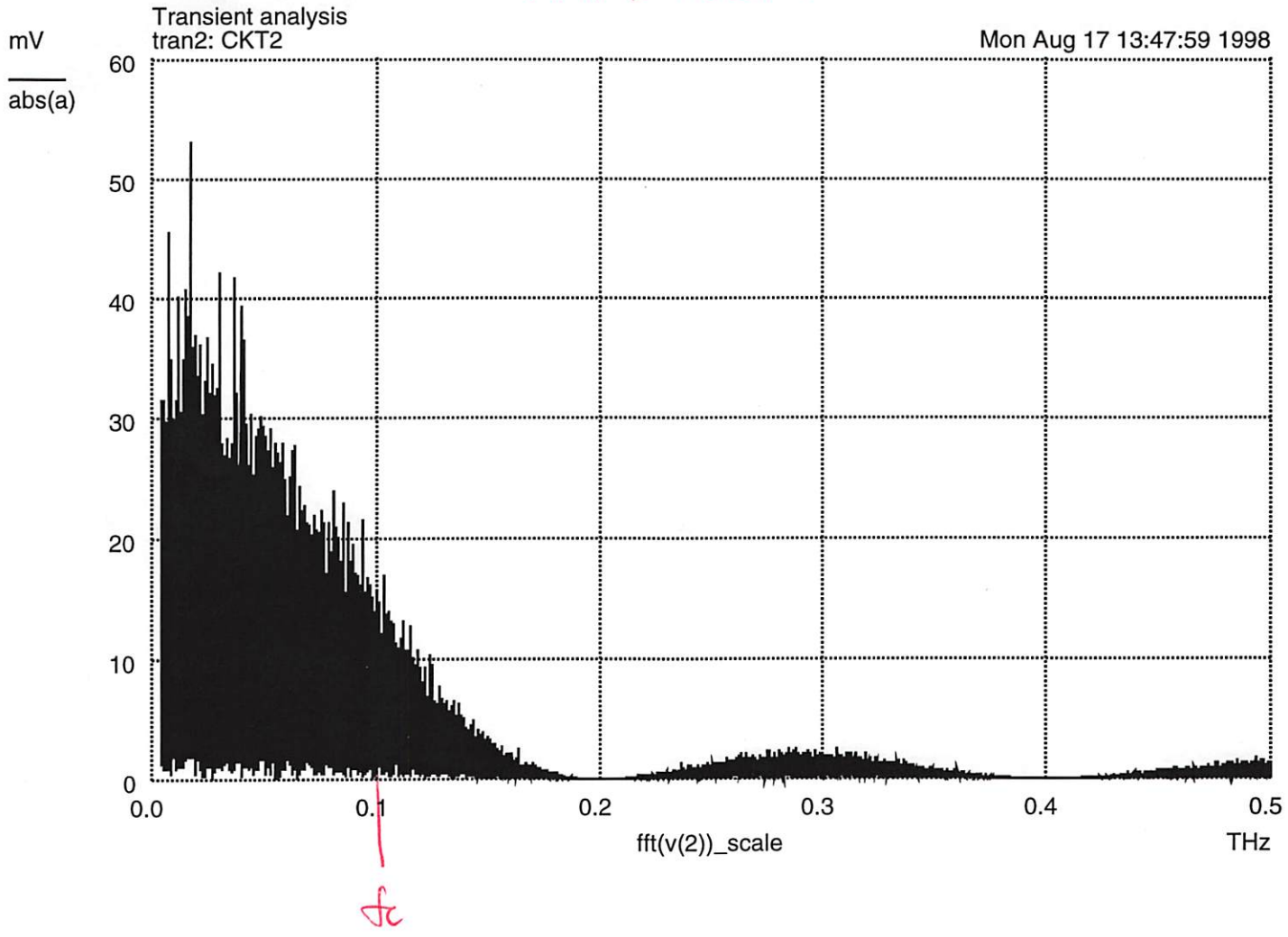

lp step

D = 5psec → f_c = 100 GHz.

Interpolated noise.

Fig. 4.

FFT : SQUARE NOISE

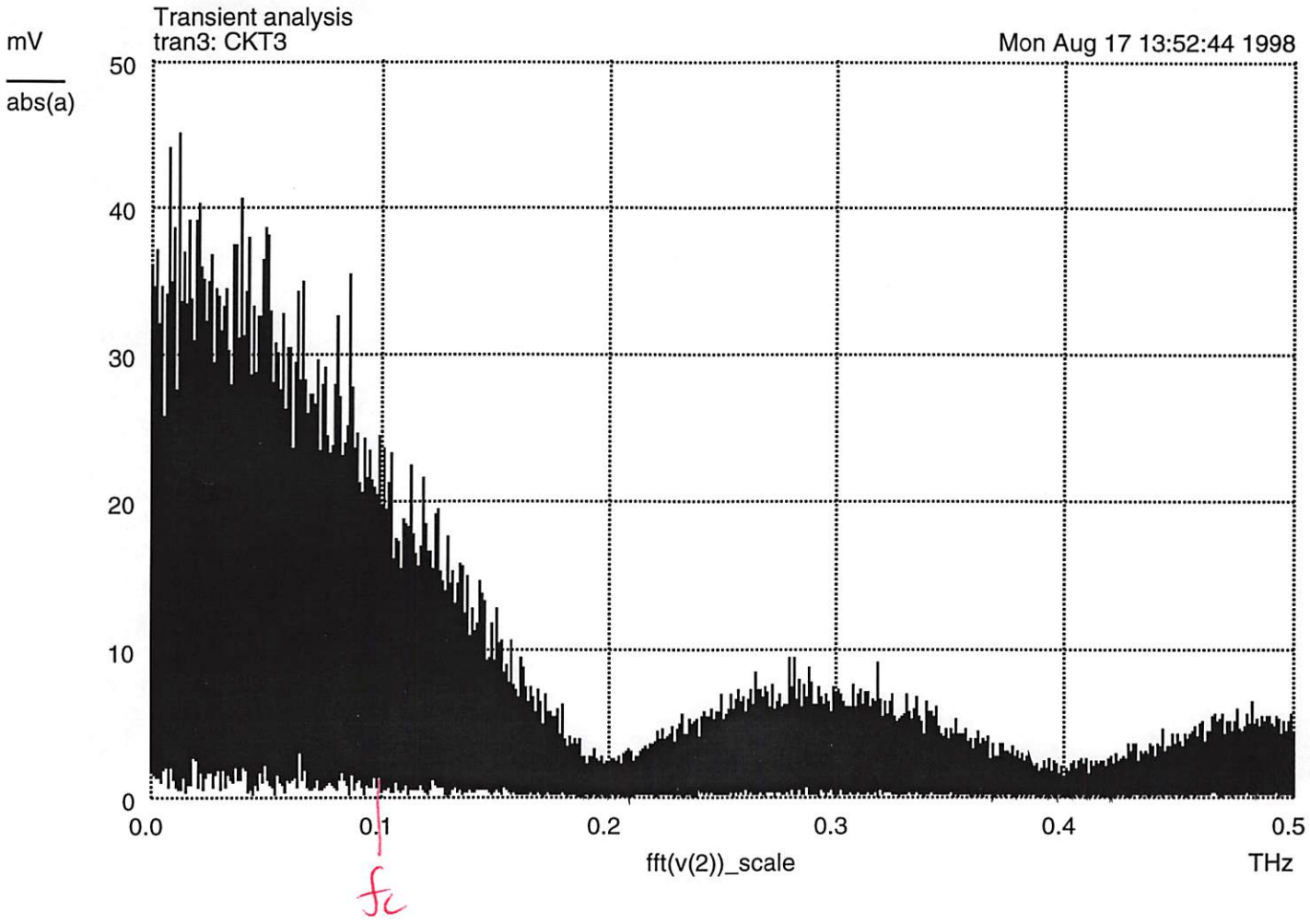

I/p step

$D = 5/sec \Rightarrow f_c = 100\,GHz = \frac{1}{2D}$

SQUARE NOISE HAS LARGER HARMONICS.

FIG. 5

FFT of filtered noise

10 GHz = f_0

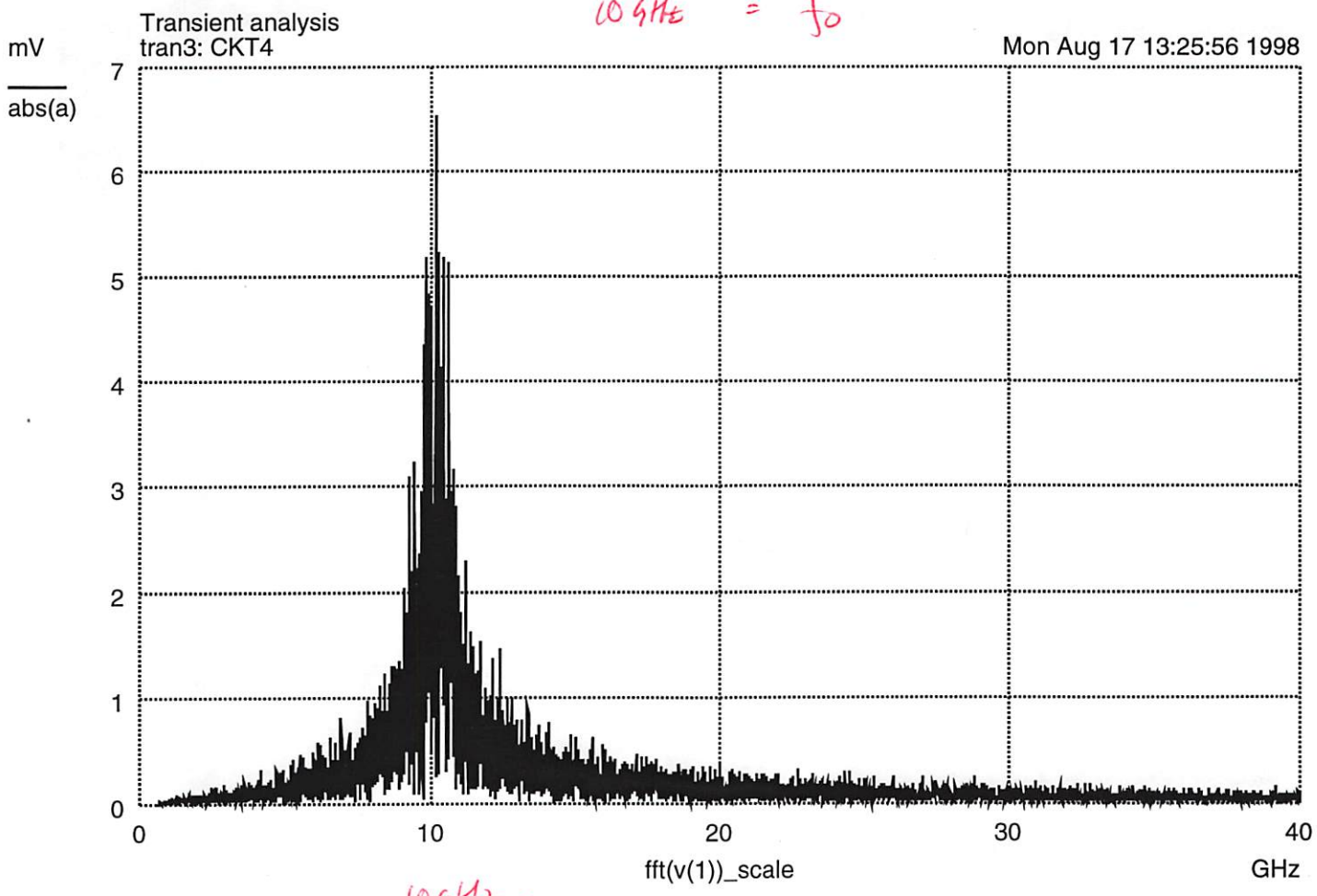

10 GHz.

f_c = 100 GHz

Fig. 6.

Junction phase and output voltage with noise

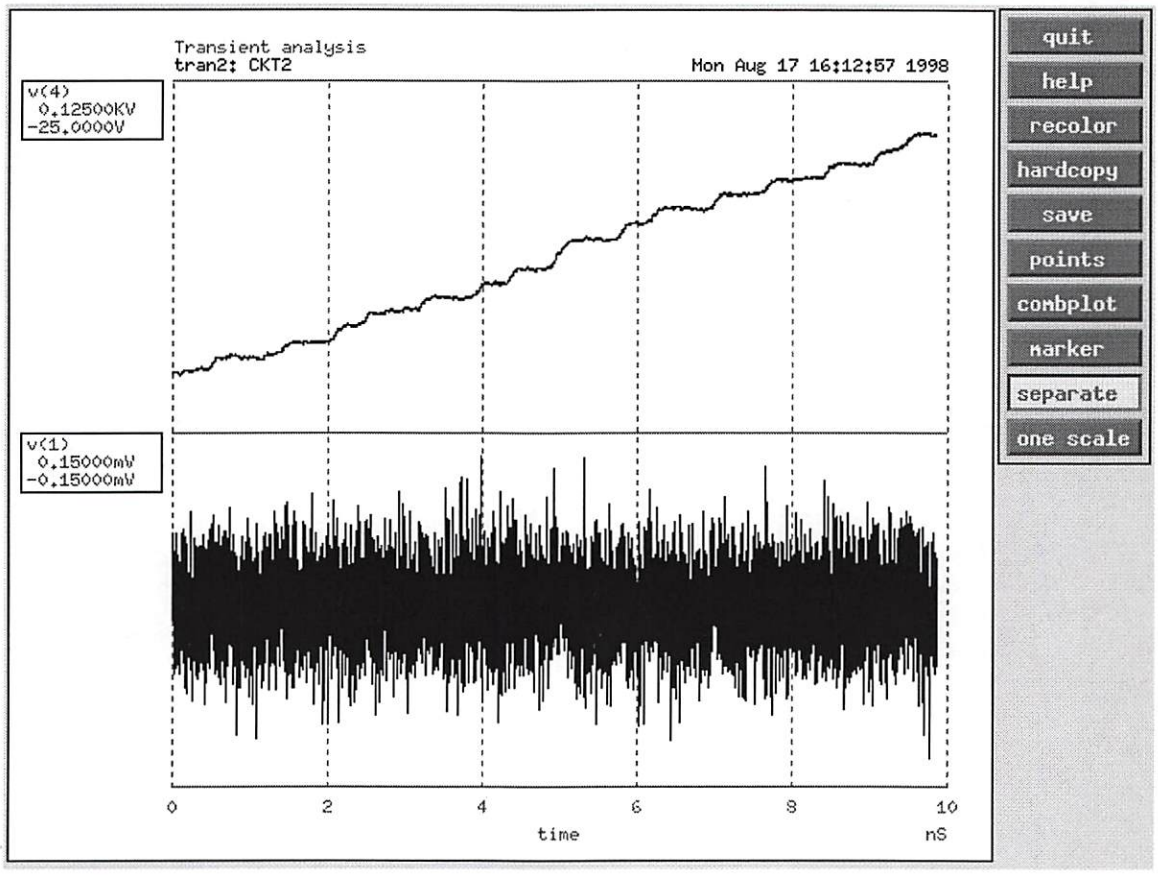

$I_c = 10\ \mu A$, $I_{bias} = 9\ \mu A$, $T = 47.78\ K$, $\gamma = 10$

Fig. 7.

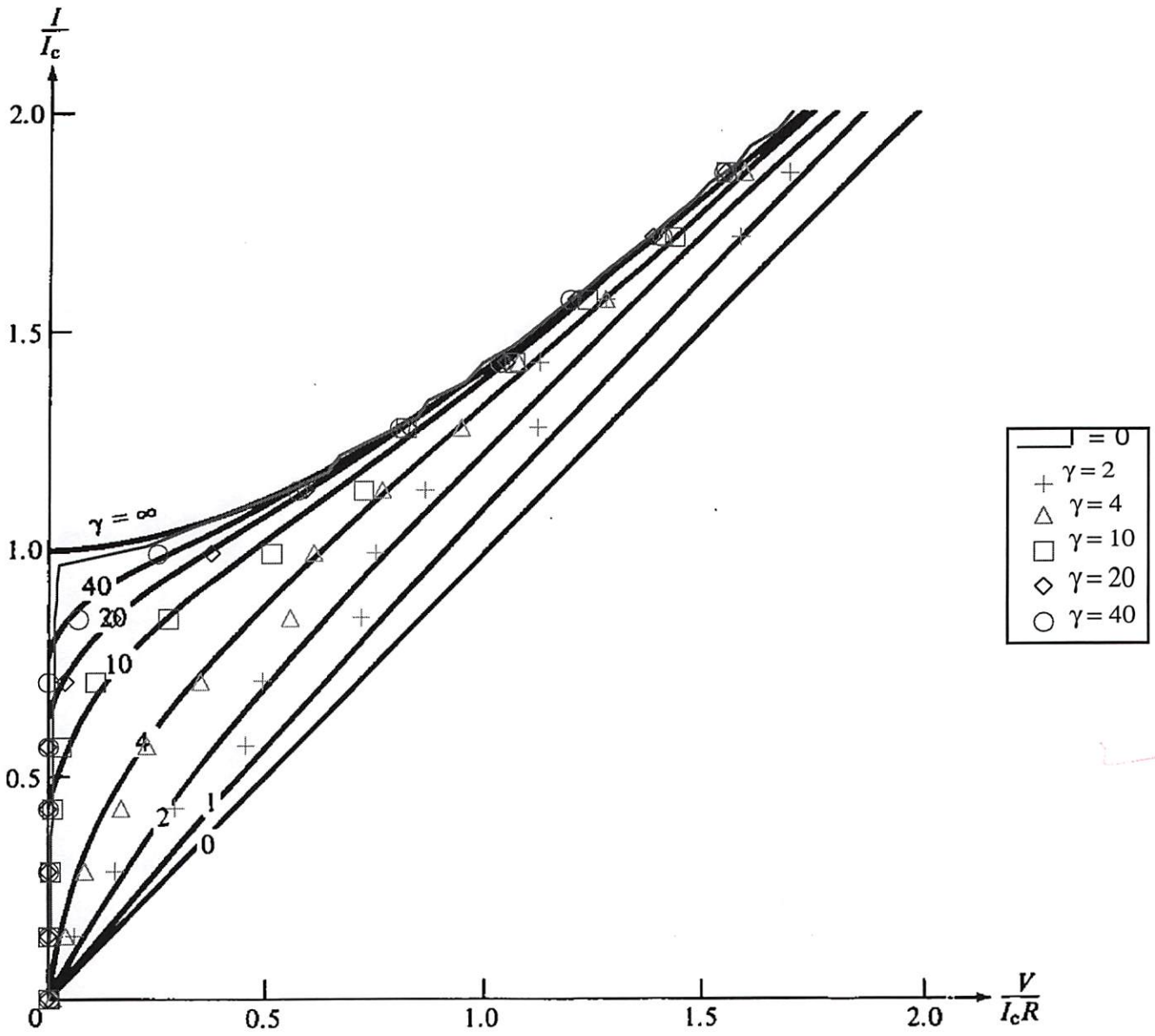

Average time interval per point = 50 ns

Fig. 8.

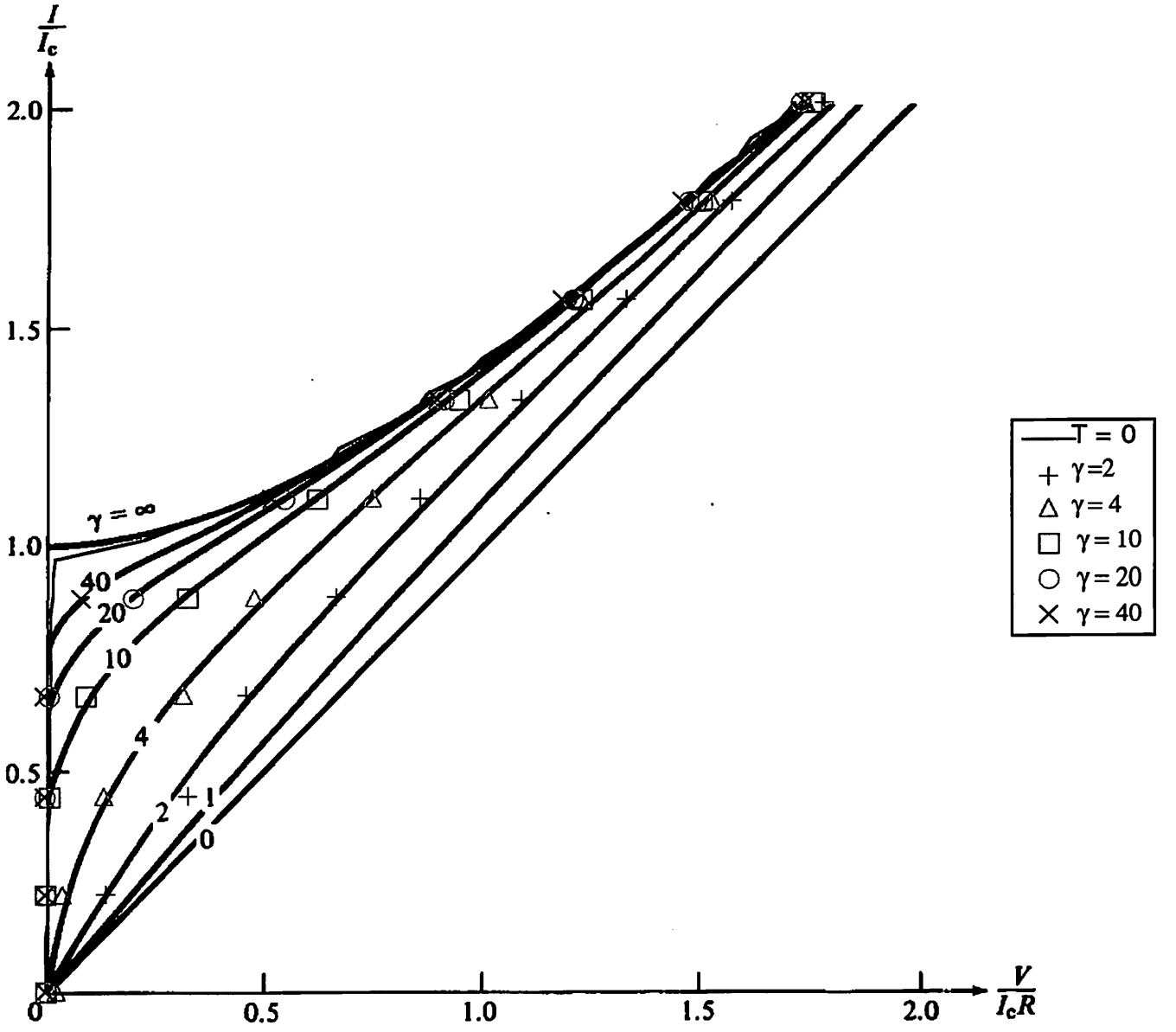

Average time interval per point = 100 ns

Fig. 9.

Script file for calculating IV rounding

```
comment
.control

let  xx = 0
while  (xx  <=0.002)
  jjwgam2.sp
  tran 1p 100n
  echo $&(mean(v(2)))  $&(mean(v(1))) >> gamma2.out
  xx = xx + 0.0002222
end

let  xx = 0
while  (xx  <=0.002)
  jjwgam4.sp
  tran 1p 100n
  echo $&(mean(v(2)))  $&(mean(v(1))) >> gamma4.out
  xx = xx + 0.0002222
end

let  xx = 0
while  (xx  <=0.002)
  jjwgam10.sp
  tran 1p 100n
  echo $&(mean(v(2)))  $&(mean(v(1))) >> gamma10.out
  xx = xx + 0.0002222
end

let  xx = 0
while  (xx  <=0.002)
  jjwgam20.sp
  tran 1p 100n
  echo $&(mean(v(2)))  $&(mean(v(1))) >> gamma20.out
  xx = xx + 0.0002222
end

let  xx = 0
while  (xx  <=0.002)
  jjwgam40.sp
  tran 1p 100n
  echo $&(mean(v(2)))  $&(mean(v(1))) >> gamma40.out
  xx = xx + 0.0002222
end

.endc
```

Spice file to calculate I/V rounding with thermal noise
Ic = 10 uA, R = 1 Ohm. Temp is chosen so that gamma = hbar Ic/eKT = 10

Mark Jeffery 8/98

```
* iv curve with noise
*@ define noise(r,t,dt,n) gauss(sqrt(4*boltz*t/(r*2*dt)), 0, dt, n)

.options Temp=47.789
.options Rnval=0.0625
.options Rval=1.0
* Original TRW parameters
* .options Rnval=0.469
.options tmin=1.0p
.options whichn=0
.options maxTime=1n

b1 1 0 4 ybco4 area=0.0625
*b1 1 0 jj1 control=v2
*v1 2 0 pwl(0 0 10n 100m)
v1 2 0 $&xx
r1 2 1 100

v2 3 0 0.5
r2 3 0 1

I10 1 0 noise($Rval, $Temp, $tmin, $whichn)

*model jj1 jj(rtype=1,cct=1,icon=10m,vg=2.8m, delv=0.1m,icrit=0.1m,r0=100,rn=*.4902,
cap=1.14195p)

* The josephson junction model
.model ybco4 jj(rtype=1,cct=1,icon=10m,vg=28m,delv=2m,
+ icrit=0.16m,r0=$Rnval,rn=$Rnval,cap=0.05p)
*TRW rn = 0.469

*.tran 0.5p 1n
.end
```

Gamma Calculated for the Noise I/V Rounding

	ic	T		gamma	T	gama
4.78E+07	1.00E-05		4.20	1.14E+02	477.90	1.00
4.78E+07	1.00E-05		4.20	1.14E+02	238.95	2.00
4.78E+07	1.00E-05		4.20	1.14E+02	159.30	3.00
4.78E+07	1.00E-05		4.20	1.14E+02	119.47	4.00
4.78E+07	1.00E-05		4.20	1.14E+02	95.58	5.00
4.78E+07	1.00E-05		4.20	1.14E+02	47.79	10.00
4.78E+07	1.00E-05		4.20	1.14E+02	23.89	20.00
4.78E+07	1.00E-05		4.20	1.14E+02	11.95	40.00

<-- this is the T for a
given gamma when ic = 10 uA

LTAGE DUE TO THERMAL NOISE IN THE dc JOSEPHSON EFFECT

Vinay Ambegaokar*
y of Atomic and Solid State Physics, Cornell University, Ithaca, New York 14850
and
B. I. Halperin
Bell Telephone Laboratories, Murray Hill, New Jersey 07974
(Received 25 April 1969)

ects of thermal fluctuations on the dc Josephson effect in a junction of small ca- are calculated using an analogy with the Brownian motion of a particle in a orce. The results are presented in a form suitable for comparison with experi-

ufficiently close to the transi- ermal fluctuations can dis- he phases of the order pa- erconductors separated by a er. The dc Josephson[1] cur- s a noise voltage with a non- A simple kinetic theory of recently been given by Ivan- an.[2] In this note we examine htly more detailed way, ob- reasons discussed below, mewhat from those of Ref. current experimental inter- mparison with experiment satisfactory preliminary re-

on junction in series with a nce and battery, so that the being driven by a constant- equations of motion are

(1)

$\dot{\theta} - V/R + \tilde{L}(t)$. (2)

osephson condition relating e phases of the order pa- ides of the junction, and V, e. We assume that the sufficiently small so that nal magnetic fields the istributed over the area. the condition of conserva- e capacitance of the junc- num Josephson current at bsence of noise[4]; R is the on, in general a function emperatures near the may be approximated by e in the normal state[5]; noise current. For $eV < T$, to which region we restrict ourselves, the noise is thermal,[6] so that $\langle \tilde{L}(t+\tau)\tilde{L}(t)\rangle = 2R^{-1}T \times \delta(\tau)$. The problem now has three dimensionless parameters: $\gamma \equiv \hbar I_1(T)/eT$, $x \equiv I/I_1(T)$, and $\Omega \equiv RC(2eI_1/\hbar C)^{1/2}$. This last quantity is the product of the circuit time constant $RC \equiv \eta^{-1}$ and the Josephson plasma frequency ω_J.[7]

Equations (1) and (2) are illuminated by a mechanical analogy. We rewrite these equations in the form

$$\dot{\theta} = p/M, \tag{3}$$

$$\dot{p} = dU/d\theta - \eta p - L(t), \tag{4}$$

where $p = (\hbar C/2e)V$, $M = (\hbar/2e)^2 C$, $L = (\hbar/2e)\tilde{L}$, and $U = -\frac{1}{2}\gamma T(x\theta + \cos\theta)$. The problem is thus entirely equivalent to the Brownian motion of a particle of mass M in the potential U. To describe this motion we form a Fokker-Planck equation[8] for the distribution function $P(\theta, p; t)$:

$$\frac{\partial P}{\partial t} = \frac{\partial U}{\partial \theta}\frac{\partial P}{\partial p} - \frac{p}{M}\frac{\partial P}{\partial \theta} + \frac{\eta\theta}{\partial p}\left[pP + MT\frac{\partial P}{\partial p}\right]. \tag{5}$$

We restrict ourselves first to the experimentally interesting case[3] where the damping rate η is large. (A fuller discussion of this condition will be given below.) One may then use the method of Kramers[8] to reduce Eq. (5) to the Smoluchowski equation for a distribution function $\sigma(\theta, t)$ in the coordinate space alone:

$$\frac{\partial \sigma}{\partial t} = \frac{1}{\eta M}\frac{\partial}{\partial \theta}\left[\left(\frac{\partial U}{\partial \theta}\right)\sigma + T\frac{\partial \sigma}{\partial \theta}\right] \equiv -\frac{\partial w}{\partial \theta}. \tag{6}$$

We only need to consider the value of θ modulo 2π, so we may restrict θ to the interval $0 \le \theta < 2\pi$, and adjoin periodic boundary conditions to Eq. (6).

The steady-state solution of Eq. (6) must have w constant. Furthermore, if σ is normalized to unity, then w^{-1} is the average time it takes for a "particle" to diffuse one periodicity length,

i.e., the average time for a phase slippage of 2π. Thus the mean voltage is given according to (1) by

$$2e\bar{V}/\hbar = 2\pi w. \tag{7}$$

The required solution of Eq. (6) is

$$\sigma(\theta) = \frac{w\eta M}{T}\frac{f(\theta)}{f(2\pi)-f(0)}\left[f(0)\int_0^\theta \frac{d\theta'}{f(\theta')} + f(2\pi)\int_\theta^{2\pi}\frac{d\theta'}{f(\theta')}\right], \tag{8}$$

where $f(\theta) = \exp[-U(\theta)/T]$. The normalization of σ then requires that

$$v \equiv \frac{\bar{V}}{I_1 R} = \frac{4\pi}{\gamma}\left\{(e^{\pi\gamma x}-1)^{-1}\left[\int_0^{2\pi} d\theta f(\theta)\right]\left[\int_0^{2\pi} d\theta' \frac{1}{f(\theta')}\right] + \int_0^{2\pi} d\theta \int_0^{2\pi} d\theta' \frac{f(\theta)}{f(\theta')}\right\}^{-1}. \tag{9}$$

The curves plotted in Fig. 1 are obtained from a numerical integration of this formula. Analytic forms can be obtained in several limits:

$$v = x, \quad \gamma \to 0; \tag{10a}$$

$$= (x^2-1)^{1/2}, \quad \gamma \to \infty, x > 1;$$

$$= 0, \quad \gamma \to \infty, x < 1; \tag{10b}$$

$$= 2(1-x^2)^{1/2}\exp\{-\gamma[(1-x^2)^{1/2} + x\sin^{-1}x]\}\sinh\tfrac{1}{2}\pi\gamma x, \quad \gamma \text{ large}, x < 1. \tag{10c}$$

Furthermore,

$$\lim_{x\to 0}\frac{v}{x} = [I_0(\tfrac{1}{2}\gamma)]^{-2}, \tag{10d}$$

where I_0 is the modified Bessel function.

To compare our work with that of Ref. 2, we remark that the result of the latter work corresponds to dividing the right-hand side of our Eq. (10c) by Ω. The difference has a simple physical origin. In the limit of large γ and small x, one can think of the phase slippage process as corresponding to thermal activation over a high energy barrier. The barriers of Ref. 2 and this work are identical. In Ref. 2 an attempt frequency $\omega_J/2\pi$ is introduced as an ad hoc assumption. Our calculation, while not restricted to the region of high barriers, contains in this limit the prefactor shown by Kramers[8] to be appropriate to the overdamped case, i.e., an attempt frequency $\omega_J^2/(2\pi\eta) = \Omega\omega_J/2\pi$, for $x \ll 1$. (The results of Ref 2 are probably correct for the case of small damping, provided the temperature and the value of x are sufficiently small relative to the damping.)

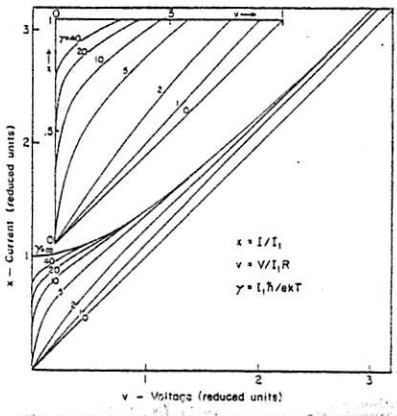

FIG. 1. Current-voltage characteristic of Josephson junction, including average noise voltage, based on Eq. (9). The inset contains an expanded version of the region $0 < x < 1$, $0 < v < 1$.

The conditions for validity of the Smoluchowski equation (6) are that the mean drift velocity of the particle be everywhere less than the thermal velocity $T^{1/2}M^{-1/2}$ and that the mean free path $T^{1/2}M^{-1/2}\eta^{-1}$ be small compared with the scale of variation in θ of the potential U. These conditions are perfectly satisfied in the limit of strong damping, $\Omega \to 0$. For Ω small but nonzero, the voltage will generally be somewhat higher than the result predicted by the Smoluchowski equation, particularly in the region $x \gtrsim 1$.

For the case of $\Omega > 1$, it becomes necessary to study the full Fokker-Planck equation (5). We hope to deal with this case in a future paper. Current-voltage curves for the Josephson junction in the absence of noise ($\gamma \to \infty$) have been discussed by McCumber and by Stewart,[9] as a function of Ω. An important qualitative feature of the

4. SQUID CHARACTERISTICS IN THE PRESENCE OF NOISE

In this section we discuss the behavior of the SQUID in the presence of Johnson noise generated in the resistive shunts. We first discuss our numerical techniques. As a check on these techniques, we show that our results for the noise-rounded i–$\bar{v}$ characteristics and voltage noise spectral densities for a single-shunted junction are in good agreement with work previously published.[15,16] We then compute the i–$\bar{v}$ characteristics, voltage noise spectral density, and flux resolution of the SQUID as functions of the relevant parameters.

4.1. Numerical Techniques

We assume that the Johnson noise voltages across the external shunt resistances dominate any other source of noise in the SQUID, for example, shot noise in the junctions[24,25] or thermal fluctuations in the critical current.[26] The voltage noise sources v_{N1} and v_{N2} in Eqs. (13)–(16) are then uncorrelated, each having a white voltage spectral density $S_V^N = 4k_BTR$, or, in dimensionless units, $S_v^N = 4\Gamma$, where[16] $\Gamma = 2\pi k_BT/I_0\phi_0$. We approximate the random voltages $v_N(\theta)$ by trains of voltage pulses each of duration $\Delta\theta$ and random amplitude v_k. We have used two different techniques to generate the v_k. In method I we generate a pseudorandom set of Gaussian-distributed v_k. We then integrate Eqs. (13)–(16) using a simple integration routine. The resultant $v(\theta)$ is used to calculate noise-rounded i–$\bar{v}$ characteristics. Unfortunately, as we shall discuss, the calculation of spectral densities from these $v(\theta)$ requires large amounts of computer time. In method II we use an approximation for the v_k that reduces significantly the computation time for the spectral densities.

Method I. We use a pseudorandom-number generator to generate a Gaussian-distributed set v_k of zero mean with $\langle v_k^2\rangle = 2\Gamma/\Delta\theta$. The computed power spectrum of the voltage pulses averaged over many sets v_k is white and tends to a constant, 4Γ, as required. Two independent trains of voltage pulses are used to approximate v_{N1} and v_{N2} in Eqs. (13)–(16). We integrate the phases $\delta_1(\theta)$ and $\delta_2(\theta)$ using an iterative scheme $\delta(\theta+\Delta\theta) = \delta(\theta)+\Delta\theta\, d\delta/d\theta$. The value of $\Delta\theta$ is chosen so that $\Delta\theta\, d\delta/d\theta \ll 2\pi$. The noise-rounded $i\bar{v}$ characteristics labeled method I in Figs. 11a and 12a and the transfer functions in Fig. 13 were generated by time-averaging $v(\theta)$ computed in this way. We estimate that the results are accurate to ±5%.

Spectral densities S_v can be calculated directly from the $v(\theta)$ generated by method I. N values of $v(\theta)$ at equal time steps $\Delta\theta$ can be used to calculate S_v at frequency intervals $\delta f = 1/(N\Delta\theta)$. For the case of a single shunt resistance ($i_c = 0$), the values of $v(\theta)$ are just the v_k, and the spectral density (averaged over many sets of v_k) tends to 4Γ as required. We shall be interested in computing spectral densities for the single junction and the SQUID from values of $v(\theta)$ sampled at time intervals corresponding to $n\,\Delta\theta$ (n is an integer). In those cases, the averaged spectral density for a single shunt resistance is white with a magnitude $n4\Gamma$. The additional factor n is a result of the normalization of the v_k. For v_k defined over time steps $\Delta\theta$, $\langle v_k^2\rangle = 2\Gamma/\Delta\theta$, while for v_k defined over $n\,\Delta\theta$, $\langle v_k^2\rangle = 2\Gamma/(n\,\Delta\theta)$. Hence, generating v_k over time steps $\Delta\theta$ and sampling the resultant $v(\theta)$ over time steps $n\,\Delta\theta$ increases the spectral density by a factor n. It is important to notice that this simple relationship will *not* hold in general for the case of the single shunted junction or SQUID, since in the limit $\Gamma \to 0$ those spectral densities must be independent of n. Hence, to obtain results for S_v that are consistent in both the noise-dominated and noise-free limits, we must take $n = 1$.

The restriction $n = 1$ limits our ability to calculate spectral densities efficiently from $v(\theta)$ when $v(\theta)$ is generated by method I. To see this, we briefly discuss the general behavior of the spectral density for $i \neq 0$, $\Gamma \neq 0$. The spectral density contains noise-broadened peaks at the fundamental Josephson frequency $f_J = \bar{v}/2\pi$ and its harmonics. We are interested in computing the low-frequency spectral density S_v^0 at frequencies well below f_J, where the spectral density is white. As the bias current i is lowered towards i_c, the harmonics become more important, and, as $\Gamma(T)$ is increased from zero, the broadening increases. Thus, for $i \sim i_c$, and for experimentally interesting values of Γ, S_v must be computed for frequencies well above and well below f_J. However, the lowest frequency is $\delta f = 1/(N\,\Delta\theta)$, where $\Delta\theta \sim 10^{-4}/f_J$. Thus $N \gg 10^4$ (for example, for $i \sim i_c$ and $\Gamma \sim 0.05$, $N \sim 10^6$), and the computation of a single spectral density is very time-consuming. In addition, many spectral densities (typically 40) must be averaged together to obtain accurate results. We thus use an alternative method to generate v_k; this method significantly reduces the computation time for spectral densities at experimentally relevant values of i and Γ.

Method II. We generate values of the Fourier transform $\tilde{v}_k$ of the Johnson noise voltages at N equal frequency intervals δf. The interval δf is fixed by the requirement $\delta f \ll f_J$, and N is fixed by the requirement $N\,\delta f \gg f_J$. The actual values of N and δf are determined empirically by computing low-frequency spectral densities S_v^0 for the SQUID for variable N and δf. The number N is increased and δf is decreased until S_v^0 becomes independent of N and δf. Typically, $N = 512$ and $\delta f = 0.01 f_J$. Our values $\tilde{v}_k$ approximate the Johnson noise in the following way. The Fourier transform of a set of Gaussian-distributed noise voltages v_k is a set of complex numbers with Gaussian-distributed amplitudes and uniformly distributed phases.[27] We approximate the Fourier transform of the noise pulses by a set of complex numbers with *constant* amplitude and uniformly distributed phases. The

amplitude of $\tilde{v}_k$ is fixed by the requirement $\langle v_k^2 \rangle = 2\Gamma N \delta f$, and the random phases are generated by a pseudorandom-number generator with uniform distribution over $[0, 2\pi]$. We find that the voltage pulse amplitudes v_k generated in this way are Gaussian-distributed. Figure 9 shows a histogram of the v_k obtained from 30 sets of $\tilde{v}_k$ in this way, together with the exact Gaussian distribution with $\langle v^2 \rangle = 2\Gamma N \delta f$. The agreement between the two curves is good. This approximation enables us to compute smooth average spectral densities for a single junction using only one set of $\tilde{v}_k$, and for the SQUID using only a small number of sets of $\tilde{v}_k$.

The Fourier transforms of the $\tilde{v}_k$ were taken as representative values of the Johnson noise over pulse times $\delta\theta = 1/(2N\delta f)$. Since $\delta\theta$ was considerably larger than the value of $\Delta\theta$ used in method I, we interpolated between adjacent noise values. We found our results for S_v^0 were independent of the details of the interpolation scheme used. Hence, we used a linear interpolation for convenience.

We found methods I and II yielded identical noise-rounded i–$\bar{v}$ characteristics for a single junction (Section 4.2). We also computed spectral densities of the voltage noise across a single junction for $i \gg i_c$ from $v(\theta)$ generated by methods I and II. The two methods yielded spectral densities

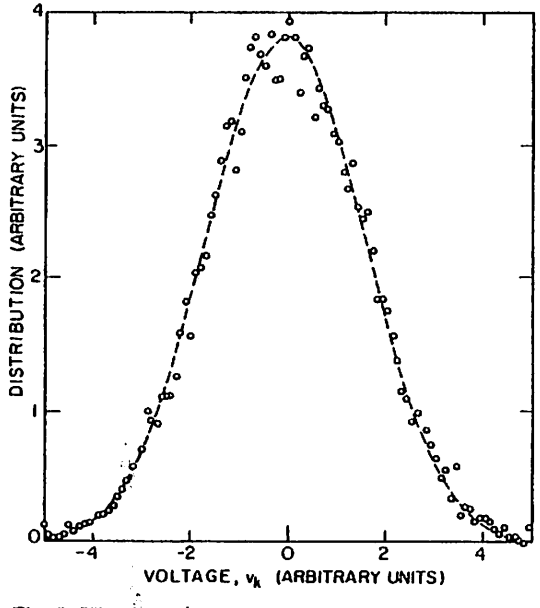

Fig. 9. Histogram of random voltages v_k generated by method II for 30 trials. Dashed curve is Gaussian with the same normalization.

that were in good agreement. However, whereas we needed to average the spectral density typically 40 times using method I, only a single set of v_k was required using method II. We also computed spectral densities using $\tilde{v}_k$ with Gaussian-distributed amplitudes. The values for S_v^0 averaged over many trials were in agrement with those obtained with constant amplitude v_k. We conclude that our approximation scheme adequately represents the Johnson noise for our purposes.

Method II was used to compute the voltage noise spectral densities of the SQUID (Fig. 14). Equations (13)–(16) were integrated with interpolated noise values determined by the v_k as in the single-junction case. We checked the values of the average voltage computed from $v(\theta)$ at time intervals $\delta\theta$ with those obtained by method I, and found good agreement. Because the SQUID involves two independent random noise sources, we found it necessary to average S_v^0 over typically eight sets of v_k to achieve a satisfactory result. We estimate that our values of S_v^0 are accurate to ±5%.

4.2. Single Junction with Noise

In order to test our numerical techniques, we first applied methods I and II of Section 4.1 to the case of a single resistively shunted Josephson junction. For a junction biased at a constant current i, the voltage v and phase δ across the junction satisfy[14]

$$v = i - \sin\delta + v_N \tag{20}$$

$$d\delta/d\theta = v \tag{21}$$

where v_N is the Johnson noise voltage across the shunt resistance. We integrated these equations stepwise in time for various values of i and Γ. Representative plots of $\delta(\theta)$ and $v(\theta)$ for $i = 0.9$ and $\Gamma = 0.05$ appear in Fig. 10. The phase $\delta(\theta)$ undergoes random excursions of considerably less than 2π about an equilibrium position for a period of time, then makes a fairly sharp transition of $+2\pi$ to an equivalent equilibrium position. These transitions are randomly timed and, according to Eq. (21), give rise to voltage pulses during the transitions. These voltage pulses are somewhat obscured in the plot of v vs. θ in Fig. 10b. The v vs. θ curve appears to be dominated by the random noise source v_N shifted by a constant voltage. This behavior is consistent with Eq. (20) since the term $(i - \sin\delta)$ is approximately constant between the transitions $\delta \to \delta + 2\pi$. Notice that, although the excursions of δ around the equilibrium positions are small compared with 2π, the time derivative $d\delta/d\theta = v$ is not small compared with the amplitude of the voltage pulses associated with the transitions in δ. In fact, as we decrease ΔT to improve our approximation for the Johnson noise source, $v \sim v_N \propto 1/\Delta T$ increases. Since the voltage pulses associated with the 2π

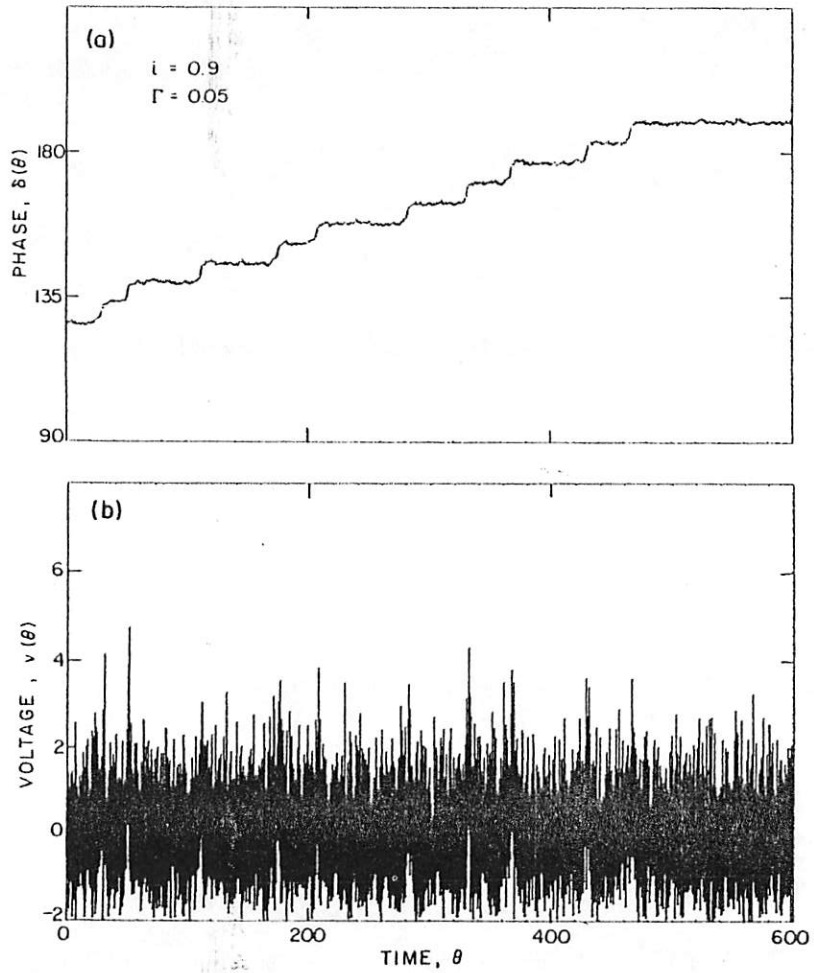

Fig. 10. Representative plots of (a) phase and (b) associated voltage vs. time for a single junction with $\Gamma = 0.05$ and $i = 0.9$.

transitions of δ have fixed area and duration, they become buried in the Johnson noise voltage pulses as T decreases.*

We obtained i–$\bar{v}$ characteristics by time-averaging $v(\theta)$ at fixed i. The i–$\bar{v}$ characteristics obtained using both methods I and II to generate $v(\theta)$ are

*Fulton[15] has used a thermal activation model in a simple derivative of the spectral density of the noise in a resistively shunted junction at currents below i_c. In this model, the noise arises from the random timing of the voltage pulses that occur when δ jumps by 2π. Although according to our calculation these pulses are obscured by the simulated Johnson noise, the results of Fulton's calculation (at low voltage), of the calculation Vystavkin *et al.*,[16] and of our calculation are all in good agreement.

shown in Fig. 11a, The smooth curves are from the Fokker–Planck calculation of Ambegaokar and Halperin.[14] The results of the two numerical techniques are in excellent agreement with each other with the Fokker–Planck calculation[14] and with other numerical calculations.[13,28]

We also computed voltage power spectral densities S_v from curves of v vs. θ using method II. We observed that the peaks in S_v corresponding to the noise-free Josephson frequency f_J and its harmonics become broadened in the presence of thermal noise. As i is reduced, the noise broadening increases in a manner that is consistent with the results of Vystavkin *et al.*[16] At frequencies well below f_J the power spectrum is white. We take the value of S_v in this region to be the low-frequency spectral density S_v^0. In Fig. 11b we plot the square root of the normalized low-frequency voltage spectral density $(S_v^0/4\Gamma)^{1/2}$ vs. the noise-rounded voltage $\bar{v}$ for two values of Γ. These values are in excellent agreement with the results of Vystavkin *et al.*[16] (obtained by another method) that are plotted as smooth curves in Fig. 11b. By comparing Figs. 11a and 11b, we observe that the maxima in $d\bar{v}/di$ and in S_v^0 occur at the same value of current, $i \approx i_c$. In addition, a decrease in the maximum of $d\bar{v}/di$ (for example, as a result of increasing Γ) is accompanied by a decrease in the maximum of S_v^0.

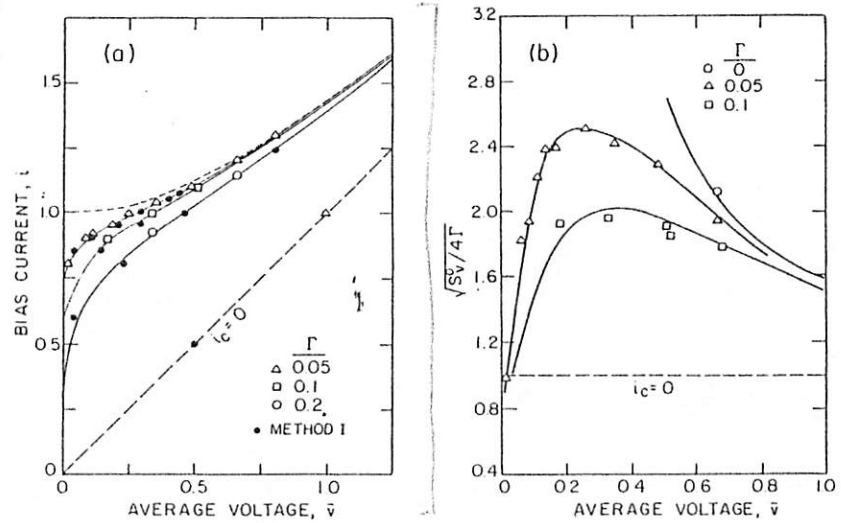

Fig. 11. (a) Current–voltage characteristics of a single resistively shunted junction in the presence of noise computed with method I (●) and method II (△, □, ○). Solid curves are from Ambegaokar and Halperin.[14] Dashed line is noise-free characteristic. (b) Low-frequency voltage spectral density vs. average voltage for a single resistively shunted junction computed with method II (△, □, ○). Solid curves are from Vystavkin *et al.*[16]

in terms of i:

$$i = (1-\alpha)\sin\delta_1 + \left\{(1+\alpha)^2 - \left[\frac{(1-\alpha)\cos\delta_1}{1+\pi\beta(1-\alpha)\cos\delta_1}\right]^2\right\}^{1/2} \quad \text{(B4)}$$

Now both F and $\partial F/\partial\delta_1$ can be expressed as function of a single variable δ_1. We search for the simultaneous zeros of F and $\partial F/\partial\delta_1$ with respect to δ_1 using a Newton–Raphson search routine in one variable only, and thus determine the maximum supercurrent i_c as a function of α, β, η, and ϕ_a.

APPENDIX C

We show that $\phi_a^\eta = \phi_a^0 - \beta\eta i/4$. Suppose the set of values (v^0, j^0, ϕ_a^0) satisfy Eqs. (13)–(16) for arbitrary α, ρ, β, and i with $\eta = 0$. We want to show that the set $(v^\eta, j^\eta, \phi_a^\eta)$ for $\eta \neq 0$ can be shifted so that the shifted values satisfy the $\eta = 0$ equations, and hence have the $\eta = 0$ time-averaged values. Now the set $(v^\eta, j^\eta, \phi_a^\eta)$ satisfy Eqs. (13)–(16) with $\eta \neq 0$. Rewriting these equations, we have

$$j^\eta = (\delta_1 - \delta_2)/\pi\beta - (\phi_a^\eta - \pi\beta i/4)2/\beta$$

and

$$v^\eta - (d\delta_1/d\theta - d\delta_2/d\theta)\eta/2 = (d\delta_1/d\theta + d\delta_2/d\theta)/2$$

Since both ϕ_a and i are independent of time, we have

$$\eta\beta\, dj^\eta/d\theta = d\delta_1/d\theta - d\delta_2/d\theta$$

Hence

$$v^\eta - (\pi\eta\beta/2)\, dj^\eta/d\theta = (d\delta_1/d\theta + d\delta_2/d\theta)/2$$

If we take $v^s = v^\eta - (\pi\eta\beta/2)\, dj^\eta/d\theta$, $j^s = j^\eta$, and $\phi_a^s = \phi_a^\eta - \pi\beta i/4$, we see that the shifted set (v^s, j^s, ϕ_a^s) satisfy Eqs. (13)–(16) for $\eta = 0$. Hence the time-averaged values $\bar{v}^s$ and $\bar{j}^s$ evaluated at ϕ_a^s will equal the original average values $\bar{v}^0$ and $\bar{j}^0$ at $\phi_a^0 = \phi_a^s$. But $j^s = j^\eta$, and $v^s = v^\eta - (\pi\eta\beta/2)\, dj^\eta/dt = v^\eta$. Hence the values v^η and j^η at some ϕ_a^η are just the values of v^0 and j^0 at $\phi_a^\eta - \eta\beta i/4$. Consequently, an imbalance η in the SQUID inductance appears as an effective external flux $-\eta\beta i/4$ for fixed bias current i.

REFERENCES

1. R. C. Jaklevic, J. Lambe, A. H. Silver, and J. E. Mercereau, *Phys. Rev. Lett.* **12**, 159 (1964); *Phys. Rev. Lett.* **14**, 887 (1965); *Phys. Rev.* **140**, A1628 (1965).
2. J. Clarke, W. M. Goubau, and M. B. Ketchen, *J. Low Temp. Phys.* **25**, 99 (1976).

3. M. Tinkham, *Introduction to Superconductivity* (McGraw-Hill, 1975), p. 214.
4. J. E. Zimmerman and A. H. Silver, *Phys. Rev.* **141**, 367 (1966).
5. E. O. Schulz-DuBois, IBM Research RZ 564 (April 13, 1973).
6. A. Th. A. M. De Waele and R. De Bruyn Ouboter, *Physica* **41**, 225 (1969).
7. A. Th. A. M. De Waele and R. De Bruyn Ouboter, *Physica* **42**, 626 (1969).
8. T. A. Fulton, *Solid State Commun.* **8**, 1353 (1970).
9. J. Clarke and J. L. Paterson, *Appl. Phys. Lett.* **19**, 469 (1971).
10. W.-T. Tsang and T. Van Duzer, *J. Appl. Phys.* **46**, 4573 (1975).
11. T. A. Fulton, L. N. Dunkleberger, and R. C. Dynes, *Phys. Rev. B* **6**, 855 (1972).
12. W.-T. Tsang and T. Van Duzer, *J. Appl. Phys.* **47**, 2656 (1976).
13. F. Auracher, Ph.D. thesis, University of California, Berkeley (1973).
14. V. Ambegaokar and B. I. Halperin, *Phys. Rev. Lett.* **22**, 1364 (1969).
15. T. A. Fulton, *IEEE Trans. Magn.* **MAG-11**, 749 (1975).
16. A. N. Vystavkin, V. N. Gubankov, L. S. Kuzmin, K. K. Likharev, V. V. Migulin, and V. K. Semenov, *Rev. Phys. Appl.* **9**, 79 (1974).
17. C. Tesche and J. Clarke, *IEEE Trans. Magn.* **MAG-13**, 859 (1977).
18. W. C. Stewart, *Appl. Phys. Lett.* **12**, 277 (1968); D. E. McCumber, *J. Appl. Phys.* **39**, 3113 (1968).
19. J. Clarke, *Phil. Mag.* **13**, 115 (1966).
20. M. B. Ketchen, W. M. Goubau, J. Clarke, and G. B. Donaldson, *IEEE Trans. Magn.* **MAG-13**, 372 (1977).
21. L. Solymar, *Superconductive Tunneling and Applications* (Chapman and Hall, London, 1972), p. 202.
22. J. Clarke and J. L. Paterson, unpublished.
23. L. G. Aslamazov, A. I. Larkin, and Yu.N. Orchinnikov, *Zh. Eksp. Teor. Fig.* **28**, 171 (1969).
24. A. J. Dahm, A. Denenstein, D. N. Langenberg, W. H. Parker, D. Rogovin, and D. J. Scalapino, *Phys. Rev. Lett.* **22**, 1416 (1969).
25. M. J. Stephen, *Phys. Rev. Lett.* **21**, 1629 (1968).
26. G. A. Hawkins and J. Clarke, *J. Appl. Phys.* **47**, 1616 (1976).
27. A. Van der Ziel, *Noise* (Prentice-Hall, New York, 1954), p. 320.
28. J. Kadlec and K. H. Gunlach, preprint.
29. S. Basaviah and J. H. Greiner, *J. Appl. Phys.* **47**, 4201 (1976).

Stochastic Simulation of SFQ Logic

Julian Satchell
DRA(Malvern), St Andrews Rd., Malvern, Worcs, WR14 3PS, United Kingdom

Abstract—**The high speed and low power of Single Flux Quantum logic (SFQ) are extremely attractive, and significant capabilities have been demonstrated in Nb technology. However the burden of cooling to 4.2K has been a barrier to its widespread implementation. The advent of High Temperature Superconductors (HTS), raises the prospect of more accessible temperatures. This paper examines some theoretical constraints on the implementation of SFQ in HTS, and derives some ideas about the parameters required of any HTS SFQ technology.**

I. Introduction

There are three obvious differences between High Temperature Superconductor (HTS) and Nb technology. First and foremost, the operating temperature will be higher, resulting in increased noise. The penetration depth is larger, leading to bigger inductances, and necessitating thicker conductors. Finally the insulator dielectric constant is much higher, so the importance of wiring capacitance in multilayer circuits is greatly increased.

The main attraction of Single Flux Quantum (SFQ) logic is its extraordinary speed power product [1]. The maximum speed scales as $I_c R_n$, and for many simple functions operation up to $f_{max} \sim I_c R_n / 3\Phi_0$ is possible. Operation of SFQ logic depends on the manipulation of flux quanta, so it is not surprising that typical inductances for the quantizing loops are in the range $L = 0.5 - 1(\Phi_0/I_c)$. When dealing with typical inductances of order a pH and currents of fractions of a mA it is convenient to rephrase the value of Φ_0 as 2.07pHmA.

The influence of capacitance on the implementation of SFQ circuits is discussed in [2].

II. Thermal Fluctuations

The natural scale of thermal current fluctuations is

$$I_n = \frac{2\pi k_B T}{\Phi_0} \qquad (1)$$

$I_n = 0.18\mu$A at 4.2K, while at 77K it has risen to $I_n = 3.2\mu$A. A typical Nb design uses $I_c = 100\mu$A, and hence inductance $L \sim 10-20$pH, depending on the circuit. This allows the circuit to work with low error rates, even if biased close to I_c, as even a bias margin of say $0.05I_c$ is much greater than I_n.

To maintain the same noise margin at 77K, we would need $I_c = 2$mA and $L \sim 0.5 - 1$pH. The critical current is marginally possible, although it is on the edge of large junction effects. The inductance is not practical, as we will see below.

III. Inductance

The primary limitation on scaling SFQ to higher temperatures comes from the relatively long penetration depth of HTS. The inductance per square for a microstrip line in the parallel plate approximation is given by

$$L_\square = \mu_0(2\lambda_L \coth \frac{t}{\lambda_L} + d) \qquad (2)$$

where t is the thickness of the superconductor layers, and d the insulator thickness.

Typical values for λ_L in high quality HTS films are $\sim$ 180nm at low temperatures ($<$ 50K), rising to 260nm at 77K. Even for the limiting case of thick films and a thin insulator $L_\square = 0.45$pH. Line capacitance forces us to use values of $d \geq \lambda_L$ [2] so $L_\square \sim 1$pH is more realistic. Note also that the dependence on t implies that it is important to work with films of more than a penetration depth in thickness.

A key topic for future study is to establish what layouts are possible for the major SFQ circuit elements. It is clearly impossible to design general multilayer circuits with 1 square inductors, although it might be allowed for special cases. It may be possible to work with a 2 square design rule, but even for this case the minimum inductor values are about $L \sim 2$pH, and so the condition for minimum inductor value $I_c L = 0.5\Phi_0$ gives $I_c = 0.5$mA.

Daly [3] has pointed out that edge junction circuits have additional stray inductance associated with the alignment tolerance of the junctions with respect to the inductor. This can easily amount to another square.

A crude estimate for the minimum practical inductance using single layer techniques is to consider a very short slot or hole, say 0.5μm in diameter. This has an inductance (estimated for $t = 300$nm, $\lambda_L = 160$nm) of $L = 2$pH, leading to a comparable limit to the multilayer case. Coupling to such small structures would be very poor, and may force the use of longer slits and hence a larger minimum inductance.

Manuscript received August 26, 1996.
Julian Satchell satchell@dra.hmg.gb

1051-8223/97$10.00

Although some very interesting and informative demonstrations of logic circuits have been made using single layer technology, it is difficult to see this as a production technology for complex circuits. Many functions require circuit crossovers, at the very least for clock and power distribution.

The unavoidable conclusion is that operation at high temperatures (around 77K) will entail some loss of noise margin, with values of I_c/T no greater than 7μA/K.

In the next section we present numerical results on four simple circuits which show that susceptibility to noise varies widely. For some circuits the noise margins used in low T_c practice are in fact needed; others will allow higher temperature operation.

IV. Stochastic Simulations

Simple analytic estimates of error rates based on activation energy arguments tend to underestimate the error rate of real circuits, as most errors occur during the complex switching transients, rather than in the quiescent state. This forces us to resort to numerical methods.

A. Methods

The results presented here have been obtained by time domain integration of the Langevin equations. The circuit simulator seeks to solve a system of equations defined by

$$dx_i = F_i(\underline{x}, t)dt + g_i dW_i(t) \qquad i = 1, N \qquad (3)$$

where the x_i are the circuit variables, F is a (nonlinear) function of those variables, g_i are constants and dW_i is the standard Weiner increment [4]. A formal solution can be obtained by integrating with respect to time,

$$x_i(t) = x_i(0) + \int_0^t F_i(\underline{x}(s), s)ds + g_i \int_0^t dW_i(s) \qquad (4)$$

This is an implicit integral equation, and to progress we make an approximation, replacing the first integral by the trapezium rule, to derive a single time step formula, which we use repeatedly. The values of the stochastic integrals $\int_0^t dW_i(s)$ can be simulated by $\xi_i\sqrt{t}$, where ξ_i are Gaussian distributed random numbers with zero mean and unit variance. This gives

$$\begin{aligned} x_i(t+\tau) = \; & x_i(t) + \tfrac{\tau}{2}\left[F_i(\underline{x}(t), t) + F_i(\underline{x}(t+\tau), t+\tau)\right] \\ & + g_i\sqrt{\tau}\xi_i(t+\tau) \end{aligned} \qquad (5)$$

Although this is still an implicit relationship, it involves only the starting and finishing times of the step. The system of nonlinear simultaneous equations that this defines can be solved by Newton-Raphson iteration (as used in Spice type simulators [5]) or fixed point iteration (JSIM)[6]. There are two main adavantages in the implicit form: stability for 'stiff' sets of equations is much improved and the convergence of the iteration provides a simple method of step size and error control.

We use a stochastic modification of JSIM, a time-domain Josephson circuit simulator developed at UCB. Unfortunateley the data structures used would make implementation of (5) very difficult. Instead we have made the substitution

$$F_i(\underline{x}(t), t) \rightarrow F_i(\underline{x}(t), t) + \frac{g_i\xi_i(t)\sqrt{2}}{\sqrt{\tau}} \qquad (6)$$

This introduces each random number twice, at the start and end of each time step. The total noise strength has been restored by the factor $\sqrt{2}$, but this is strictly only valid for linear F. In the nonlinear case, errors are introduced that increase with noise strength and step size. We can control these errors by circumventing the standard step size control mechanism in JSIM to force short steps; the relatively low computational cost of steps in JSIM reduces the penalty.

Some additional implementation details are included in the appendix.

B. Usage

Error probabilities have been estimated from ensembles of simulations, with different initializations of the random number generators. For an ensemble of N simulations and an error probability p we expect to see pN errors. When p is small Poisson statistics apply, so the variance of the number of errors is also pN. Obtaining reasonably accurate estimates of low values of p requires large ensembles, restricting studies to simple circuits.

The software system has been validated by comparing the results for a thermally rounded, low capacitance junction with the analytical solution of Ambegaokar and Halperin[7]. The agreement holds even in the extreme low voltage tail of the IV curve. The agreement is within statistical error, but if it were expressed as a difference between theoretical and simulated noise temperatures the difference would be less than 2%.

C. Circuits

Four circuits have been studied to date, listed in Table I, along with their deterministic margins for the most critical junction I_c. In all cases they are simplified and idealized, without any attempt to include the parasitics of real implementations. They are not known to be correctly optimised, and the results obtained may not be representative of the capabilities of the circuit with different optimization, or a different set of inputs and tests. In all cases the inputs and tests were chosen to be relatively

TABLE I

Circuit	Deterministic Margin (%)
Voltage Multiplier [9]	14.4
XOR gate [1]	28.5
Flip Flop [1]	35.5
Memory Cell [8]	35.5

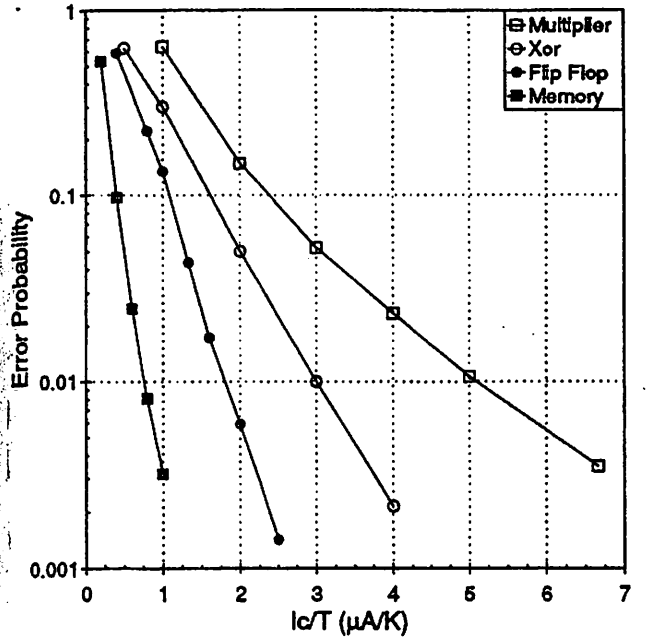

Fig. 1. Arrhenius plots of error probability against I_c/T.

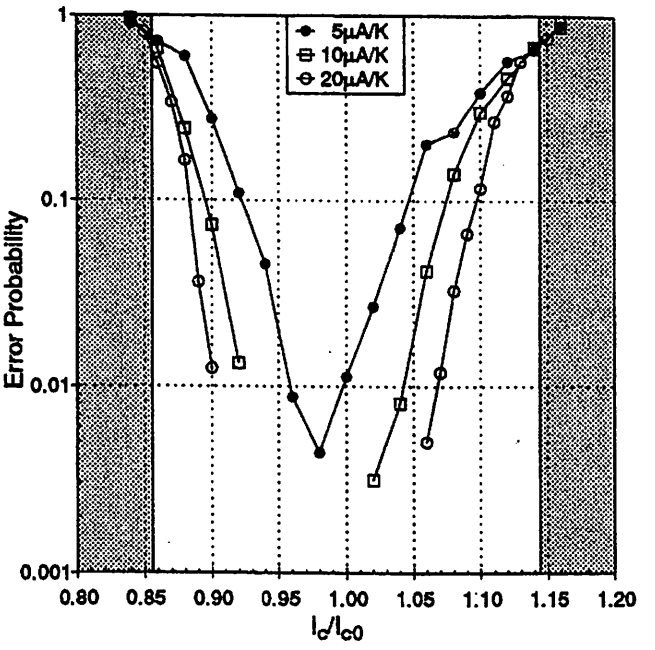

Fig. 2. Effect of junction tolerance for voltage multiplier at three different values of I_c/T. The shaded regions correspond to the deterministic margins.

slow, so the circuits attained a quasi static state between switching events. The memory cell has been studied using an array of three cells, writing to and reading from the center cell. This reduces boundary artifacts. The margins calculations below are for the case where the cells are kept identical. Single cell margins appear to bigger than those quoted, probably because of bias current redistribution between neighbouring cells. The references in Table I contain schematics. The actual circuit files used in the simulations could be supplied by e-mail on request.

D. Results

We studied the temperature dependence of the error probability for the nominal design. The error probabilities vary strongly with temperature, as expected. Fig. 1 shows that for all the circuits, the error probability can be approximated by the form

$$\ln p = A - B\frac{I_c}{T} \tag{7}$$

This is a type of generalised Arrhenius relation[10]. We can use it to extrapolate to the much lower error probabilities required in many applications.

Examining the time domain data at high error rates shows that the overwhelming majority of errors occur at switching transients, even though the circuits are being tested quasi-statically. As the error rate is therefore proportional to switching rate, an error probability is more useful than a rate. For sufficiently low switching rates, the errors would presumably become dominated by thermally activated changes of state.

Table II summarizes the data from Fig. 1. The value of I_c/T needed to attain an arbitrary error probability of 10^{-12} is also listed. The values range from barely attainable even for Helium temperature technology, to rather easy for 77K operation. This leads to our most important conclusion; circuits differ enormously in their noise tolerance. Some are viable for high temperature operation, others are not.

The results shown so far are for the circuits at their nominal design center values. Present day HTS junction technology suffers from relatively poor reproducibility of I_c, and circuits will in general be fabricated with non ideal critical currents. The production yield falls rapidly as complexity rises unless the margins are significantly wider than the standard deviation of I_c. Noise causes margin narrowing. When a circuit is operated with parameters which lie inside the region of deterministic success, it may still have such a high error rate that it is not useful. We have studied the effect of deviations from the nominal design values on the error probability. Figs. 2 and 3 show data for the two extreme cases of the voltage multiplier (noise sensitive) and the memory (noise resistant) respectively.

The voltage multiplier (in the form simulated) is extremely noise sensitive. The region of correct operation is small without noise, and even small amounts of noise narrow it further. Some applications of the voltage multi-

TABLE II

Circuit	A	B(K/μA)	I_c/T (μA/K)
Voltage Multiplier	-1.05	0.68	39.7
XOR gate	0.51	1.83	16.7
Flip Flop	0.9	2.99	4.8
Memory Cell	0.0	5.76	9.5

Fits for Arrhenius equation. A and B are the slope and offset parameters of (7). The value of I_c/T needed to attain an arbitrary target value of 10^{-12} is listed in the last column.

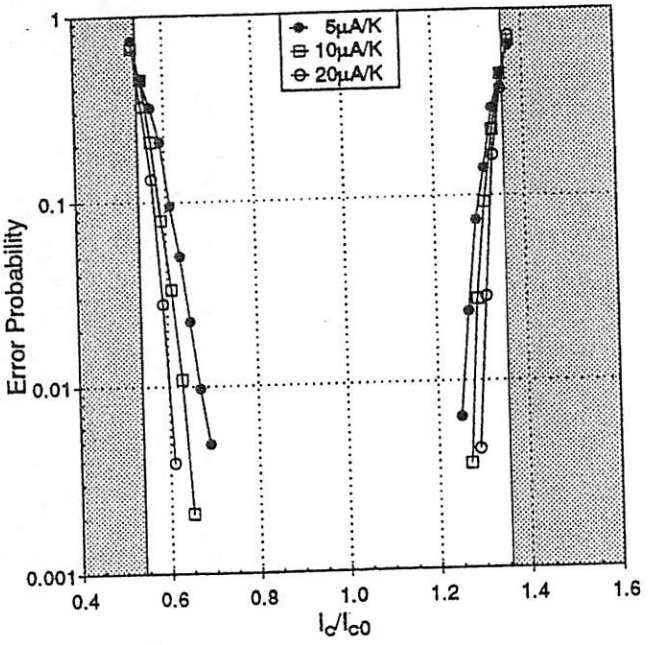

Fig. 3. Effect of junction tolerance for memory at three different values of I_c/T. The shaded regions correspond to the deterministic margins. Note that the horizontal axes are different from the previous figure.

plier can tolerate many errors; for example if it were used as a SQUID preamplifier errors only add slightly to the noise level. In these cases this effect may not be so severe as to preclude use.

The SFQ memory cell has excellent noise resistance, and suffers only mildly from noise induced margin narrowing. Even if we extrapolate the lines on Fig. 3 to much lower error probabilities, the margins remain wide enough that the circuit still looks manufacturable.

The contrast between the two cases is extreme. Deterministic margins do not seem to be a reliable indicator of noise resistance, as evidenced by the much better noise tolerance of the memory cell than the flip flop, despite the similar deterministic margins. At present it appears that extensive numerical studies are needed for candidate HTS circuits. When more circuits have been examined it may be possible to extract more general principles, and these should prove an invaluable guide to the design of SFQ circuits for HTS.

V. Conclusions

We have seen above that inductance limits the usable values of I_c to be no more than about 0.5mA. Low T_c practice corresponds to $25-50\mu AK^{-1}$. This is needed for some circuits, which fixes the maximum attainable operating temperature as no more than 20K.

Operation at significantly higher temperatures is only possible for those circuits which have good noise tolerance. A number of SFQ functions exist which are extremely robust. The invention of new circuit implementations to widen the list of such functions is seen to be the critical field of endeavour for the future of SFQ in high temperature superconductors.

Appendix

Two additional JSIM device types have been defined to implement current and voltage noise sources. No provision has been made for noise in non-linear resistors (the g_i in (3) are constants), but this is not needed for the high T_c case. In practice the simulator is used with an *awk* script which modifies a noiseless circuit for simulation at finite temperature by adding current noise sources in parallel with any resistors. Test criteria are embedded in the circuit file in the form of JSIM comments, and these appear in the output stream. The format of these comments is defined below, and we offer this format as a possible standard for those using JSIM.

An auxiliary programme parses the tests, and halts the simulation if any condition is violated; this means that files with multiple tests are subject to statistical depletion at high error rates, as most of the simulations fail on an early test.

The test criteria are defined by lines of the form

*TEST*n time minimum maximum*

The opening asterisk labels the line as a comment to JSIM, which passes it through to the output stream. The ouput variable to test is specified by an integer n, followed by real numbers specifying the time, and minimum and maximum values.

References

[1] K. K. Likharev and V. K. Semenov, *IEEE Trans. Appl. Superconductivity*, vol. 1, pp. 3-28, March 1991.

[2] J. Satchell, "Is HTS Usable for SFQ Logic?", *Proceedings of the 3rd Workshop on Digital Applications, Josephson Junctions and 3-Terminal Devices* University of Twente, Netherlands, April 1996, in press.

[3] K. Daly, TRW, Redondo Beach, Los Angeles Ca., personal communication, 1996.

[4] C. W. Gardiner, *Handbook of Stochastic Methods* Berlin: Springer-Verlag, 1983.

[5] L. Nagel, "A Computer Program to Simulate Semiconductor Circuits", Memo no. ERL-M520, ERL, EECS Dept. University of California, Berkely, 1975.

[6] E. Fang and T. Van Duzer, *Extended Abstracts of 1989 International Superconductivity Conference (ISEC'89)*, pp. 407-410, June 1989, Tokyo.

[7] V. Ambegaokar and B. I. Halperin, *Phys. Rev. Lett.*, vol. 22, pp. 1364, June 1969.

[8] S. V. Polonsky, A. F. Kirichenko, V. K. Semenov and K. K. Likharev, *IEEE Trans. Appl. Superconductivity* , vol. 5, pp. 3000-3004, June 1995.

[9] V. K. Kaplunenko, H. R. Yi, B. Nilsson, T. Claeson and E. Wikborg, *Inst. Phys. Conf. Ser. No.* 148, pp. 1657-1660, 1995.

[10] H. Toepfer and F. H. Uhlmann, *Inst. Phys. Conf. Ser. No.* 148, pp. 1721-1724, 1995.

Numerical Recipes in C

The Art of Scientific Computing

William H. Press
Harvard-Smithsonian Center for Astrophysics

Brian P. Flannery
EXXON Research and Engineering Company

Saul A. Teukolsky
Department of Physics, Cornell University

William T. Vetterling
Polaroid Corporation

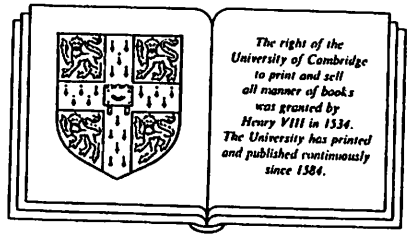

CAMBRIDGE UNIVERSITY PRESS
Cambridge
New York Port Chester

Chapter 12. Fourier Transform Spectral Methods

12.0 Introduction

A very large class of important computational problems falls under the general rubric of "Fourier transform methods" or "spectral methods." For some of these problems, the Fourier transform is simply an efficient computational tool for accomplishing certain common manipulations of data. In other cases, we have problems for which the Fourier transform (or the related "power spectrum") is itself of intrinsic interest. These two kinds of problems share a common methodology.

Largely for historical reasons the literature on Fourier and spectral methods has been disjoint from the literature on "classical" numerical analysis. In this day and age there is no justification for such a split. Fourier methods are commonplace in research and we shall not treat them as specialized or arcane. At the same time, we realize that many computer users have had relatively less experience with this field than with, say, differential equations or numerical integration. Therefore our summary of analytical results will be more complete. Numerical algorithms, per se, begin in §12.2.

A physical process can be described either in the *time domain*, by the values of some quantity h as a function of time t, e.g. $h(t)$, or else in the *frequency domain*, where the process is specified by giving its amplitude H (generally a complex number indicating phase also) as a function of frequency f, that is $H(f)$, with $-\infty < f < \infty$. For many purposes it is useful to think of $h(t)$ and $H(f)$ as being two different *representations* of the *same* function. One goes back and forth between these two representations by means of the *Fourier transform* equations,

$$H(f) = \int_{-\infty}^{\infty} h(t) e^{2\pi i f t} dt$$
$$h(t) = \int_{-\infty}^{\infty} H(f) e^{-2\pi i f t} df \tag{12.0.1}$$

If t is measured in seconds, then f in equation (12.0.1) is in cycles per second, or Hertz (the unit of frequency). However, the equations work with

other units. If h is a function of position x (in meters), H will be a function of inverse wavelength (cycles per meter), and so on. If you are trained as a physicist or mathematician, you are probably more used to using *angular frequency* ω, which is given in *radians* per sec. The relation between ω and f, $H(\omega)$ and $H(f)$ is

$$\omega \equiv 2\pi f \qquad H(\omega) \equiv [H(f)]_{f=\omega/2\pi} \tag{12.0.2}$$

and equation (12.0.1) looks like this

$$H(\omega) = \int_{-\infty}^{\infty} h(t) e^{i\omega t} dt$$
$$h(t) = \frac{1}{2\pi} \int_{-\infty}^{\infty} H(\omega) e^{-i\omega t} d\omega \tag{12.0.3}$$

We were raised on the ω-convention, but we changed! There are fewer factors of 2π to remember if you use the f-convention, especially when we get to discretely sampled data in §12.1.

From equation (12.0.1) it is evident at once that Fourier transformation is a *linear* operation. The transform of the sum of two functions is equal to the sum of the transforms. The transform of a constant times a function is that same constant times the transform of the function.

In the time domain, function $h(t)$ may happen to have one or more special symmetries It might be *purely real* or *purely imaginary* or it might be *even*, $h(t) = h(-t)$, or *odd*, $h(t) = -h(-t)$. In the frequency domain, these symmetries lead to relationships between $H(f)$ and $H(-f)$. The following table gives the correspondence between symmetries in the two domains:

If...	then...
$h(t)$ is real	$H(-f) = [H(f)]^*$
$h(t)$ is imaginary	$H(-f) = -[H(f)]^*$
$h(t)$ is even	$H(-f) = H(f)$ [i.e. $H(f)$ is even]
$h(t)$ is odd	$H(-f) = -H(f)$ [i.e. $H(f)$ is odd]
$h(t)$ is real and even	$H(f)$ is real and even
$h(t)$ is real and odd	$H(f)$ is imaginary and odd
$h(t)$ is imaginary and even	$H(f)$ is imaginary and even
$h(t)$ is imaginary and odd	$H(f)$ is real and odd

In subsequent sections we shall see how to use these symmetries to increase computational efficiency.

Here are some other elementary properties of the Fourier transform. (We'll use the "$\Longleftrightarrow$" symbol to indicate transform pairs.) If

$$h(t) \Longleftrightarrow H(f)$$

$$h(at) \Longleftrightarrow \frac{1}{|a|} H\left(\frac{f}{a}\right) \qquad \text{"time scaling"} \tag{12.0.4}$$

$$\frac{1}{|b|} h\left(\frac{t}{b}\right) \Longleftrightarrow H(bf) \qquad \text{"frequency scaling"} \tag{12.0.5}$$

$$h(t - t_0) \Longleftrightarrow H(f)\, e^{2\pi i f t_0} \qquad \text{"time shifting"} \tag{12.0.6}$$

$$h(t)\, e^{-2\pi i f_0 t} \Longleftrightarrow H(f - f_0) \qquad \text{"frequency shifting"} \tag{12.0.7}$$

With two functions $h(t)$ and $g(t)$, and their corresponding Fourier transforms $H(f)$ and $G(f)$, we can form two combinations of special interest. The *convolution* of the two functions, denoted $g * h$, is defined by

$$g * h \equiv \int_{-\infty}^{\infty} g(\tau) h(t - \tau)\, d\tau \tag{12.0.8}$$

Note that $g * h$ is a function in the time domain and that $g * h = h * g$. It turns out that the function $g * h$ is one member of a simple transform pair

$$g * h \Longleftrightarrow G(f) H(f) \qquad \text{"Convolution Theorem"} \tag{12.0.9}$$

In other words, the Fourier transform of the convolution is just the product of the individual Fourier transforms.

The *correlation* of two functions, denoted $\mathrm{Corr}(g, h)$, is defined by

$$\mathrm{Corr}(g, h) \equiv \int_{-\infty}^{\infty} g(\tau + t) h(\tau)\, d\tau \tag{12.0.10}$$

The correlation is a function of t, which is called the *lag*. It therefore lies in the time domain, and it turns out to be one member of the transform pair:

$$\mathrm{Corr}(g, h) \Longleftrightarrow G(f) H^*(f) \qquad \text{"Correlation Theorem"} \tag{12.0.11}$$

[More generally, the second member of the pair is $G(f)H(-f)$, but we are restricting ourselves to the usual case in which g and h are real functions, so we take the liberty of setting $H(-f) = H^*(f)$.] This result shows that multiplying the Fourier transform of one function by the complex conjugate of the Fourier Transform of the other gives the Fourier transform of their correlation. The correlation of a function with itself is called its *autocorrelation*. In this case (12.0.11) becomes the transform pair

$$\mathrm{Corr}(g, g) \Longleftrightarrow |G(f)|^2 \qquad \text{"Wiener-Khinchin Theorem"} \tag{12.0.12}$$

The *total power* in a signal is the same whether we compute it in the time domain or in the frequency domain. This result is known as *Parseval's theorem*:

$$\text{Total Power} \equiv \int_{-\infty}^{\infty} |h(t)|^2\, dt = \int_{-\infty}^{\infty} |H(f)|^2\, df \tag{12.0.13}$$

Frequently one wants to know "how much power" is contained in the frequency interval between f and $f + df$. In such circumstances one does not usually distinguish between positive and negative f, but rather regards f as varying from 0 ("zero frequency" or D.C.) to $+\infty$. In such cases, one defines the *one-sided power spectral density (PSD)* of the function h as

$$P_h(f) \equiv |H(f)|^2 + |H(-f)|^2 \qquad 0 \le f < \infty \tag{12.0.14}$$

so that the total power is just the integral of $P_h(f)$ from $f = 0$ to $f = \infty$. When the function $h(t)$ is real, then the two terms in (12.0.14) are equal, so $P_h(f) = 2|H(f)|^2$. Be warned that one occasionally sees PSDs defined without this factor two. These, strictly speaking, are called *two-sided power spectral densities*, but some books are not careful about stating whether one- or two-sided is to be assumed. We will always use the one-sided density given by equation (12.0.14). Figure 12.0.1 contrasts the two conventions.

If the function $h(t)$ goes endlessly from $-\infty < t < \infty$, then its total power and power spectral density will, in general, be infinite. Of interest then is the *(one- or two-sided) power spectral density per unit time*. This is computed by taking a long, but finite, stretch of the function $h(t)$, computing its PSD [that is, the PSD of a function which equals $h(t)$ in the finite stretch but is zero everywhere else], and then dividing the resulting PSD by the length of the stretch used. Parseval's theorem in this case states that the integral of the one-sided PSD-per-unit-time over positive frequency is equal to the mean-square amplitude of the signal $h(t)$.

You might well worry about how the PSD-per-unit-time, which is a function of frequency f, converges as one evaluates it using longer and longer stretches of data. This interesting question is the content of the subject of "power spectrum estimation," and will be considered below in §12.8–§12.9. A crude answer for now is: the PSD-per-unit-time converges to finite values at all frequencies *except* those where $h(t)$ has a discrete sine-wave (or cosine-wave) component of finite amplitude. At those frequencies, it becomes a delta-function, i.e. a sharp spike, whose width gets narrower and narrower, but whose area converges to be the mean-square amplitude of the discrete sine or cosine component at that frequency.

We have by now stated all of the analytical formalism that we will need in this chapter with one exception: In computational work, especially with experimental data, we are almost never given a continuous function $h(t)$ to work with, but are given, rather, a list of measurements of $h(t_i)$ for a discrete

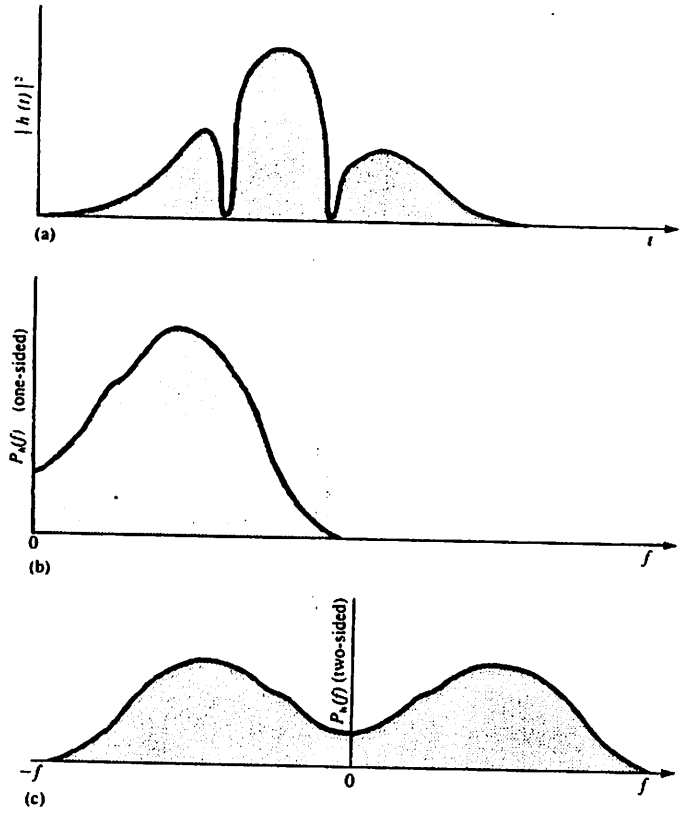

Figure 12.0.1 Normalizations of one- and two-sided power spectra. The area under the square of the function, (a), equals the area under its one-sided power spectrum at positive frequencies, (b), and also equals the area under its two-sided power spectrum at positive and negative frequencies, (c).

set of t_i's. The profound implications of this seemingly unimportant fact are the subject of the next section.

REFERENCES AND FURTHER READING:

Champeney, D.C. 1973, *Fourier Transforms and Their Physical Applications* (New York: Academic Press).

Elliott, D.F., and Rao, K.R. 1982, *Fast Transforms: Algorithms, Analyses, Applications* (New York: Academic Press).

12.1 Fourier Transform of Discretely Sampled Data

In the most common situations, function $h(t)$ is sampled (i.e., its value is recorded) at evenly spaced intervals in time. Let Δ denote the time interval between consecutive samples, so that the sequence of sampled values is

$$h_n = h(n\Delta) \qquad n = \ldots, -3, -2, -1, 0, 1, 2, 3, \ldots \tag{12.1.1}$$

The reciprocal of the time interval Δ is called the *sampling rate*; if Δ is measured in seconds, for example, then the sampling rate is the number of samples recorded per second.

Sampling Theorem and Aliasing

For any sampling interval Δ, there is also a special frequency f_c, called the *Nyquist critical frequency*, given by

$$f_c \equiv \frac{1}{2\Delta} \tag{12.1.2}$$

If a sine wave of the Nyquist critical frequency is sampled at its positive peak value, then the next sample will be at its negative trough value, the sample after that at the positive peak again, and so on. Expressed otherwise: *Critical sampling of a sine wave is two sample points per cycle.* One frequently chooses to measure time in units of the sampling interval Δ. In this case the Nyquist critical frequency is just the constant 1/2.

The Nyquist critical frequency is important for two related, but distinct, reasons. One is good news, and the other bad news. First the good news. It is the remarkable fact known as the *sampling theorem*: If a continuous function $h(t)$, sampled at an interval Δ, happens to be *band-width limited* to frequencies smaller in magnitude than f_c, i.e., if $H(f) = 0$ for all $|f| > f_c$, then the function $h(t)$ is *completely determined* by its samples h_n. In fact, $h(t)$ is given explicitly by the formula

$$h(t) = \Delta \sum_{n=-\infty}^{+\infty} h_n \frac{\sin[2\pi f_c(t - n\Delta)]}{\pi(t - n\Delta)} \tag{12.1.3}$$

This is a remarkable theorem for many reasons, among them that it shows that the "information content" of a band-width limited function is, in some sense, infinitely smaller than that of a general continuous function. Fairly often, one is dealing with a signal which is known on physical grounds to be band-width limited (or at least approximately band-width limited). For example, the signal may have passed through an amplifier with a known, finite